iScience

CellPress

Article

Androgen Receptor Is a Non-canonical Inhibitor of Wild-Type and Mutant Estrogen Receptors in Hormone Receptor-Positive Breast Cancers

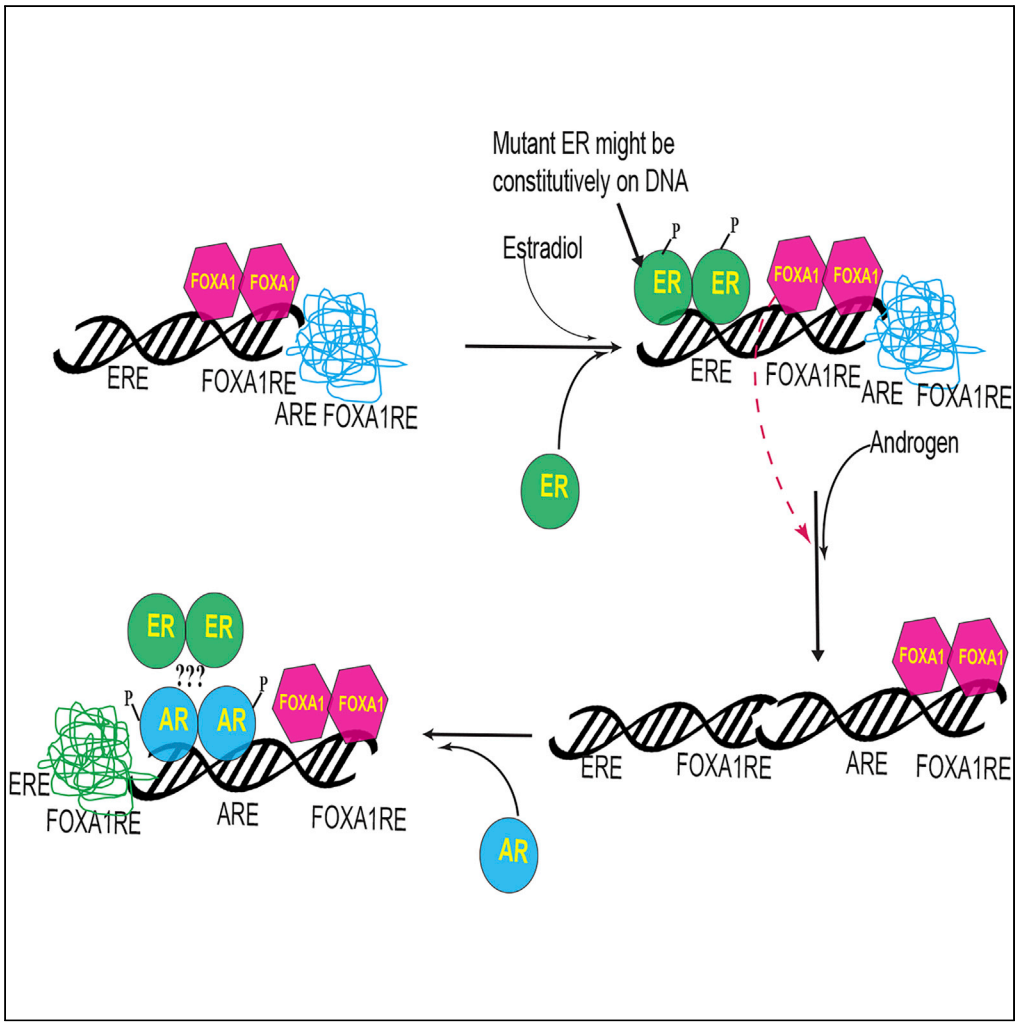

Suriyan Ponnusamy, Sarah Asemota, Lee S. Schwartzberg, ..., Emanuel F. Petricoin, Henry W. Long, Ramesh Narayanan

rnaraya4@uthsc.edu

HIGHLIGHTS

Androgen receptor (AR) agonists inhibit estrogen receptor (ER)-positive breast cancer

Activating AR reprograms ER and FOXA1 cistrome, resulting in ER inhibition

AR agonist alters the phosphoproteome signature consistent with growth inhibition

Ponnusamy et al., iScience 21, 341–358
November 22, 2019
https://doi.org/10.1016/j.isci.2019.10.038

iScience

CellPress

Article

Androgen Receptor Is a Non-canonical Inhibitor of Wild-Type and Mutant Estrogen Receptors in Hormone Receptor-Positive Breast Cancers

Suriyan Ponnusamy,[1] Sarah Asemota,[1] Lee S. Schwartzberg,[2] Fouzia Guestini,[3] Keely M. McNamara,[3] Mariaelena Pierobon,[4] Alba Font-Tello,[5] Xintao Qiu,[5] Yingtian Xie,[5] Prakash K. Rao,[5] Thirumagal Thiyagarajan,[1] Brandy Grimes,[2] Daniel L. Johnson,[6] Martin D. Fleming,[1] Frances E. Pritchard,[1] Michael P. Berry,[2] Roy Oswaks,[2] Richard E. Fine,[2] Myles Brown,[5] Hironobu Sasano,[3] Emanuel F. Petricoin,[4] Henry W. Long,[5] and Ramesh Narayanan[1,2,7,*]

SUMMARY

Sustained treatment of estrogen receptor (ER)-positive breast cancer with ER-targeting drugs results in ER mutations and refractory unresponsive cancers. Androgen receptor (AR), which is expressed in 80%–95% of ER-positive breast cancers, could serve as an alternate therapeutic target. Although AR agonists were used in the past to treat breast cancer, their use is currently infrequent due to virilizing side effects. Discovery of tissue-selective AR modulators (SARMs) has renewed interest in using AR agonists to treat breast cancer. Using translational models, we show that AR agonist and SARM, but not antagonist, inhibit the proliferation and growth of ER-positive breast cancer cells, patient-derived tissues, and patient-derived xenografts (PDX). Ligand-activated AR inhibits wild-type and mutant ER activity by reprogramming the ER and FOXA1 cistrome and rendering tumor growth inhibition. These findings suggest that ligand-activated AR may function as a non-canonical inhibitor of ER and that AR agonists may offer a safe and effective treatment for ER-positive breast cancer.

INTRODUCTION

Worldwide, over 2 million women were diagnosed with breast cancer in 2018, and over 600,000 died of breast cancer (Bray et al., 2018). In the United States, an estimated 266,000 women were diagnosed and approximately 40,000 women died from breast cancer in 2018 (Siegel et al., 2018). Estrogen receptor-α (ER)-positive breast cancer subtype constitutes the majority of breast cancers. ER plays an important role in classifying breast cancer, in defining proliferative characteristics, and in developing a treatment regimen (Andersen and Poulsen, 1989; Musgrove and Sutherland, 2009; Perou et al., 2000; Rossi et al., 2015).

ER is a ligand-dependent transcription factor that is predominantly activated by estrogens. ER-positive breast cancers that are dependent on ER for growth are treated with ER antagonists or inhibitors of estradiol-synthesizing enzyme, aromatase (AI) (Eastell et al., 2008; Robertson et al., 2013; Vogel et al., 2006). Compared with ER-negative or triple-negative breast cancer (TNBC), ER-positive breast cancers typically have a lower proliferation index and a well-differentiated phenotype (Heise and Gorlich, 1982; Neifeld et al., 1982; Perou et al., 2000; Stewart et al., 1982). Women suffering from ER-positive breast cancers suffer from osteoporosis, muscle wasting, and poor quality of life, resulting from extended ER blockade.

Prolonged treatment of cancers with inhibitors or antagonists results in mutations in the target protein and activation of resistance pathways (Balbas et al., 2013; Hara et al., 2003; Sasaki et al., 2011). For example, continued treatment of ER-positive breast cancers with ER antagonists or AI results in resistance, often due to mutations in the ER ligand-binding domain (LBD) (Fuqua et al., 1993; Karnik et al., 1994; Musgrove and Sutherland, 2009; Robinson et al., 2013). Clinical studies have estimated that over 30% of breast cancers treated with tamoxifen become refractory and recur as a resistant cancer and over 40% of recurrent breast cancers express mutated ER (Chandarlapaty et al., 2016; Early Breast Cancer Trialists' Collaborative et al., 2015; Magnani et al., 2017). Mutant ERs that have escaped the hormonal axis and have become hormone independent fail to respond to endocrine therapy, and, consequently, these patients will need to be

[1]Department of Medicine, College of Medicine, University of Tennessee Health Science Center, 19, S. Manassas, Room 120, Memphis, TN 38103, USA

[2]West Cancer Center, Memphis, TN, USA

[3]Department of Pathology, Tohoku University Graduate School of Medicine, Sendai, Japan

[4]Center for Applied Proteomics and Molecular Medicine, George Mason University, Manassas, VA, USA

[5]Center for Functional Cancer Epigenetics, Dana-Farber Cancer Institute, Boston, MA, USA

[6]Molecular Informatics Core, University of Tennessee Health Science Center, Memphis, TN, USA

[7]Lead Contact

*Correspondence: rnaraya4@uthsc.edu

https://doi.org/10.1016/j.isci.2019.10.038

treated with cell cycle inhibitors such as CDK4/6 inhibitors or cytotoxic agents. Such cancers require new non- or less-toxic effective endocrine therapies.

Androgen receptor (AR) is expressed in over 80%–90% of ER-positive breast cancer (Collins et al., 2011; Garay and Park, 2012; Hu et al., 2011; Narita et al., 2006; Niemeier et al., 2010). Until ER-targeted treatment options were made available, breast cancer was treated with steroidal androgens such as dihydrotestosterone (DHT) (Adair and Herrmann, 1946; Kennedy, 1958) or even with estrogens such as diethylstilbestrol (DES) (Gordan et al., 1963). AR expression in ER-positive breast cancer is associated with improved overall survival (OS) and disease-free survival (DFS) (Vera-Badillo et al., 2014). Studies have shown that co-expression of AR and steroidogenic enzymes such as 5-α-reductase that synthesize active DHT correlated with better progression-free survival (PFS) and OS (Sultana et al., 2014). Other evidences suggest that the AR may increase breast cancer growth or even have a role in the development of tamoxifen resistance (Barton et al., 2017; Bronte et al., 2018; Ciupek et al., 2015; Danforth et al., 2010; De Amicis et al., 2010; Kaaks et al., 2005; Liao and Dickson, 2002).

Recent preclinical and clinical studies indicate that AR could be a growth promoter in tamoxifen-resistant breast cancer, but a growth inhibitor in tamoxifen-sensitive breast cancer. Although AR antagonist enzalutamide increased proliferation of parental breast cancer cell line MCF-7, it inhibited proliferation of tamoxifen-resistant MCF-7 cells (Creevey et al., 2019). Similarly, tamoxifen-resistant clinical specimens that had higher AR:ER ratio had aggressive disease and poor prognosis (Cao et al., 2019). On the contrary, AR-positive ER-positive breast cancer had smaller tumors, better prognosis, lower tumor grade, and better disease-free survival after chemotherapy (Aleskandarany et al., 2016; Witzel et al., 2013). Preclinical studies in parental MCF-7 and ZR-75-1 cells demonstrated antiproliferative effects with AR agonists (Kandouz et al., 1999; Poulin et al., 1988). These conflicting evidences from literature can be comprehensively resolved using translational patient-derived tissues and controlled clinical trials.

In this study, we found that proliferation and growth of patient-derived xenografts (PDX) and tissues that express wild-type and mutant ER were inhibited by AR agonist and tissue-selective AR modulator (SARM) (Dalton et al., 1998) but not by an AR antagonist. Ligand-activated AR inhibited growth of these tumors by reprogramming the ER and FOXA1 cistrome and by altering the phosphokinome signature, resulting in inhibition of ER function. Overall, the results provide an evidence for a tumor suppressive role for ligand-activated AR and create an opportunity to treat ER-positive breast cancer with a less-toxic hormonal approach.

RESULTS

The SARM enobosarm (GTx-024 or ostarine) is an AR agonist that binds to and activates the AR with EC_{50} at less than 10 nM (Narayanan et al., 2014; Ponnusamy et al., 2017b). Enobosarm was evaluated in clinical trials and was shown to increase lean mass and physical function without having significant virilizing side effects (Crawford et al., 2016; Dalton et al., 2011; Dobs et al., 2013). Preclinical studies described in this manuscript were conducted with a non-metabolizable SARM to eliminate any confounding results obtained due to potential metabolism of steroidal androgens into weaker androgen or estrogen metabolites (Jin and Penning, 2001; Oliveira et al., 2007). Moreover, clinical trials have shown enobosarm to be an effective treatment for breast cancer (https://finance.yahoo.com/news/gtx-announces-top-line-results-120000738.html, 2018; Overmoyer, 2015).

SARM Inhibits Breast Cancer Cell Proliferation

To determine the role of AR in breast cancer, we analyzed the TCGA dataset for survival of breast cancer patients expressing higher vs lower AR (Figure 1A). Kaplan-Meier plot of the TCGA dataset demonstrated that breast cancer patients expressing higher AR correlated with longer survival than patients with breast cancer expressing lower AR (hazard ratio of 0.52 and log rank P of 1.1 e−10). This suggests that AR expression might have a beneficial role in breast cancer. Further analysis of the dataset suggested that patients with luminal A and B breast cancers expressing higher AR had a significantly improved survival, whereas ER-negative breast cancer patients had no significant survival benefit.

We conducted studies using various preclinical and translational models to understand the role of AR and its mechanism of action in ER-positive breast cancer. Proliferation of ZR-75-1 cells that express AR and ER

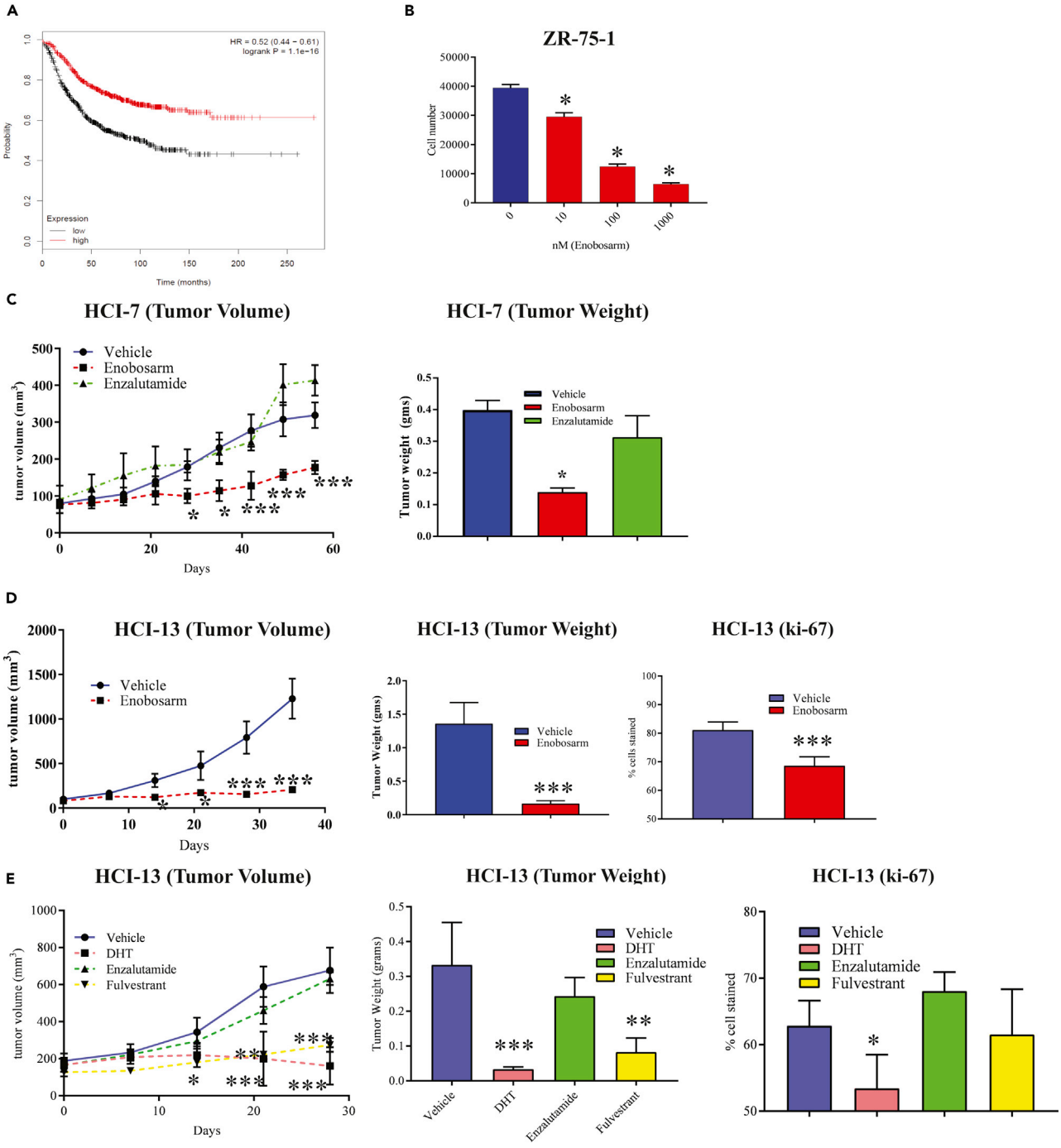

Figure 1. AR Agonist Inhibits Proliferation and Growth of Wild-Type and Mutant ER-positive Xenograts

(A) Higher AR expression correlates with patient survival. Patients who have high or low expression of AR in the TCGA dataset were compared for survival. Hazard ratio = 0.52 (0.44–0.61). Log rank P = 1.1×10^{-16}.

(B) Enobosarm inhibits the proliferation of ZR-75-1 cells. ZR-75-1 breast cancer cells plated in growth medium (n = 4/treatment) were treated with indicated doses of enobosarm for 12 days, with medium changed and re-treated every third day. After 12 days of treatment, cells were harvested, and the number of cells was counted.

(C) Enobosarm inhibits HCI-7 tumor growth. HCI-7 PDX was surgically implanted as 1 mm^3 fragments under the mammary fat pad in NSG female mice (n = 6-10/group) that were ovariectomized and supplemented with estradiol. Once the tumors reached 100–200 mm^3, the mice were randomized and treated with vehicle (DMSO:PEG-300 (15%:85%)), enobosarm (10 mpk p.o.), or enzalutamide (30 mpk p.o.). Tumor volume was measured weekly. At sacrifice, tumors were removed, weighed (right panel), and stored for further analysis.

Figure 1. *Continued*

(D) Enobosarm inhibits growth of HCI-13 PDX. HCI-13 PDX was surgically implanted as 1 mm^3 fragments under the mammary fat pad in intact female NSG mice (n = 6-10/group). Once the tumors reached 100–200 mm^3, the mice were randomized and treated with vehicle (DMSO:PEG-300 (15%:85%)) or enobosarm (10 mpk p.o.). Tumor volume was measured weekly. At sacrifice, tumors were removed, weighed (middle panel), and stored for further analysis. Tumors that were stored in formalin were further processed and immunohistochemistry was performed for the proliferation marker Ki-67 (right panel).

(E) AR agonist DHT inhibits growth of *HCI-13 PDX*. HCI-13 PDX was performed as indicated above. The mice were randomized and treated with vehicle (DMSO:PEG-300 (15%:85%)), DHT (10 mpk s.c.), or enzalutamide (30 mpk p.o.), or fulvestrant (200 mpk s.c. twice weekly). Tumor volume was measured twice weekly. At sacrifice, tumors were removed, weighed (middle panel), and stored for further analysis. Ki-67 was performed in formalin-fixed paraffin-embedded tumors (right panel).

* = $p < 0.05$; ** = $p < 0.01$; *** = $p < 0.001$. HCI, Huntsman Cancer Institute; AR, androgen receptor; ER, estrogen receptor; NSG, NOD SCID Gamma; PDX, patient-derived xenograft; OVX, ovariectomy; mpk, milligram per kilogram body weight; DHT, dihydrotestosterone.

was reduced dose-dependently by the AR agonist enobosarm after twelve days of treatment, providing an evidence for anti-proliferative effects of an AR agonist in ER-positive breast cancer (Figure 1B).

Enobosarm Inhibits Wild-Type ER-positive Breast Cancer PDX Growth

Enobosarm was tested in a PDX expressing wild-type ER. From the numerous PDXs available in Dr. Alana Welm's laboratory (DeRose et al., 2011), we identified two ER-positive AR-positive PDXs, HCI-7 and HCI-13 (Table S1; Figure S1 top blot; HCI-9 is an ER-negative AR-positive PDX). HCI-7 tumor fragments were implanted under the mammary fat pad of female NSG mice that were ovariectomized and supplemented with an estradiol pellet. Once the tumors reached 100–200 mm^3, the mice were randomized and treated orally with vehicle, 10 mg/kg enobosarm, or 30 mg/kg enzalutamide. The enzalutamide dose was selected based on previously published data (Cochrane et al., 2014; D'Amato et al., 2016; Park et al., 2016; Pollock et al., 2016). The growth and tumor weight (measured at the conclusion of the study) of HCI-7 were inhibited significantly by enobosarm but not by enzalutamide (Figure 1C). Immunohistochemistry staining of the HCI-7 tumors confirmed ER and AR expression and also significant inhibition of proliferation marker Ki-67 in enobosarm-treated tumors (Figure S1).

One characteristic of AR agonists, but not antagonists, is their ability to stabilize AR protein expression (Kemppainen et al., 1992; Zhou et al., 1995). We used AR expression to ensure that enobosarm behaved as an agonist in our PDXs. Results show that AR was stabilized by enobosarm in HCI-7 tumors, indicating that the tumors were exposed to enobosarm and that enobosarm behaved as an agonist (Figure S1).

As the presence of integral murine-stromal cellular infiltration is an issue in PDXs that have undergone passages in immunodeficient mouse strains, we chose Ku80 as a marker for human epithelial cells and H&E evaluation as an approach to quantifying murine stromal content and human epithelial cells (Allard et al., 2014; Maykel et al., 2014; Schneeberger et al., 2016; Tentler et al., 2012). These stains clearly enable us to differentiate between the epithelial and stromal cells and will provide us with the percentage of different cell types present in the PDXs. Ku80 and H&E staining showed that the tumors have predominantly epithelial cells with minimal mouse stromal infiltration in a ratio of around 91:9% of epithelial:stromal cells (Figure S1).

AR Agonist Inhibits Growth of Mutant ER-positive PDX

We discovered by internal sequencing as well as from literature that HCI-13 (an invasive lobular breast cancer) PDX expresses an ER that is mutated in the LBD at Y537 (Sikora et al., 2014). This mutation frequently occurs in ER-positive breast cancers that have been treated with ER antagonists or aromatase inhibitors (Jeselsohn et al., 2018; Toy et al., 2017). HCI-13 was obtained from a patient who was treated with and relapsed from drugs ranging from ER-targeted therapeutics to chemotherapy (Table S1).

To determine if an AR agonist will have the ability to inhibit growth of a mutant ER-positive breast cancer, HCI-13 tumor fragments were implanted under the mammary fat pad in NSG mice. Once the tumors attained 100–200 mm^3, the animals were randomized and treated with vehicle or enobosarm. Enobosarm significantly inhibited growth (Figure 1D left), tumor weights (Figure 1D middle), and Ki-67 (Figure 1D right).

We conducted additional xenograft studies with HCI-13 tumors where the animals were treated with steroidal androgen, DHT (10 mg/kg/day subcutaneously), competitive AR antagonist, enzalutamide (30 mg/kg/day orally), and the ER degrader, fulvestrant (200 mg/kg/twice weekly subcutaneously) (Guo et al., 2018). Consistent with the effect of a SARM, DHT significantly inhibited tumor growth, whereas

the AR antagonist enzalutamide failed to inhibit tumors (Figure 1E left). Fulvestrant also inhibited tumor growth significantly. Tumor weights recorded at the end of the study, and Ki67 confirmed the results observed in tumor growth (Figure 1E middle and right).

We measured drug concentration in the serum of animals treated with various drugs using standardized LC-MS/MS methods. Steady-state drug concentrations were above their target engagement concentration, suggesting that drug exposure was not a limiting factor in HCI-13 tumor-bearing animals (Figure S2A).

H&E and Ku80 staining indicated that the HCI-13 tumors have tumor epithelial cells with limited mouse stromal cell infiltration (84:16) (Figure S2B). For all tumors (HCI-7 and 13), morphology observed via H&E was within the range typical of breast carcinoma.

Ex Vivo Culture with Tumor Specimens Indicates Heterogeneity of Response to ER and AR Ligands

Breast cancer is heterogeneous in its genomic profile as well as in its response to treatments. To determine the effect of enobosarm and fulvestrant on growth inhibition, we cultured breast cancer specimens obtained from patients, on dental sponges. These patient specimens were collected as indicated in the methods under an Institutional Review Board (IRB) approval. The characteristics of these patient specimens are provided in Table S1. Specimens were treated with vehicle, 1 μM enobosarm, or 100 nM fulvestrant. Three days after treatment, RNA was isolated from the tissues and expression of ER- and AR-target genes was measured (Figure S2C). Expression of ER and AR was confirmed using immunohistochemistry. All the specimens, except specimen 1,075, express the two targets with greater than 80% expression observed (Figure S3). Fulvestrant inhibited the ER function as measured by the expression of pS2 in five of eight specimens, whereas enobosarm inhibited the ER function in three of eight specimens (Figure S2C). FKBP5, an AR-target gene, was used to ensure that the AR in these tumors was functional.

Enobosarm Inhibits HCI-13 Breast Cancer Growth by Inhibiting ER Function

To determine global gene-expression pattern in response to enobosarm, RNA from HCI-13 tumors was subjected to Affymetrix microarray. In total, 3,029 genes were differentially regulated by enobosarm in HCI-13 tumors compared with vehicle-treated tumors. Enobosarm upregulated 1,792 genes and downregulated 1,237 genes. Heatmap of the differentially regulated genes clearly indicates a shift in the expression pattern of genes due to enobosarm treatment (Figure 2A).

Ingenuity pathway analysis (IPA) showed that the ER-target genes were highly enriched followed by the AR-target genes in enobosarm-treated specimens (p values of 6.66^{-11} vs 2.83^{-7}; Figure 2C). A subset of the ER-target genes was down-regulated by enobosarm, whereas all the AR-target genes were up-regulated (Figure 2B). Although ER-target genes such as *TFF1*, *PGR*, *GREB1*, and *NRIP1* were down-regulated by enobosarm, other ER-target genes such as *CTSD* and *CCND1* were not inhibited by enobosarm. These results provide evidence that enobosarm functions in breast cancer by at least partially inhibiting the ER-signaling pathway to reduce cancer growth.

The genes enriched for the AR pathway were fed into TCGA database to determine the consequence of altering the AR pathway by an AR agonist. AR pathway genes correlated with a significant increase in survival of breast cancer patients (hazard ratio of 0.64 and log rank P of 1.1×10^{-8}) (Figure 2D).

To ensure that enobosarm is not an ER antagonist and the effects are mediated through AR, an ER competitive ligand binding assay (Figure S4A) and an ER transactivation assay (Figure S4B) were performed. Both results indicate that enobosarm has no direct interaction with ER, which is in concordance with earlier published results (Yin et al., 2003).

Chromatin Immunoprecipitation-Sequencing (ChIP-Seq) Analysis Demonstrates that Enobosarm Reprograms ER and AR Cistromes

To determine if the effect of enobosarm on ER function is due to any direct effect on ER binding to DNA, ChIP-sequencing for ER was performed in the tumor samples obtained from animals shown in Figure 1D. ER binding to 1,148 regions ($q < 0.05$) on the DNA was reprogrammed by enobosarm, with 572 regions statistically enriched with ER and 576 regions depleted of ER (Figure 3A), whereas Principal component analysis (PCA) (Figure 3B) and unsupervised hierarchical clustering (Figure 3D) show the distinct distribution of

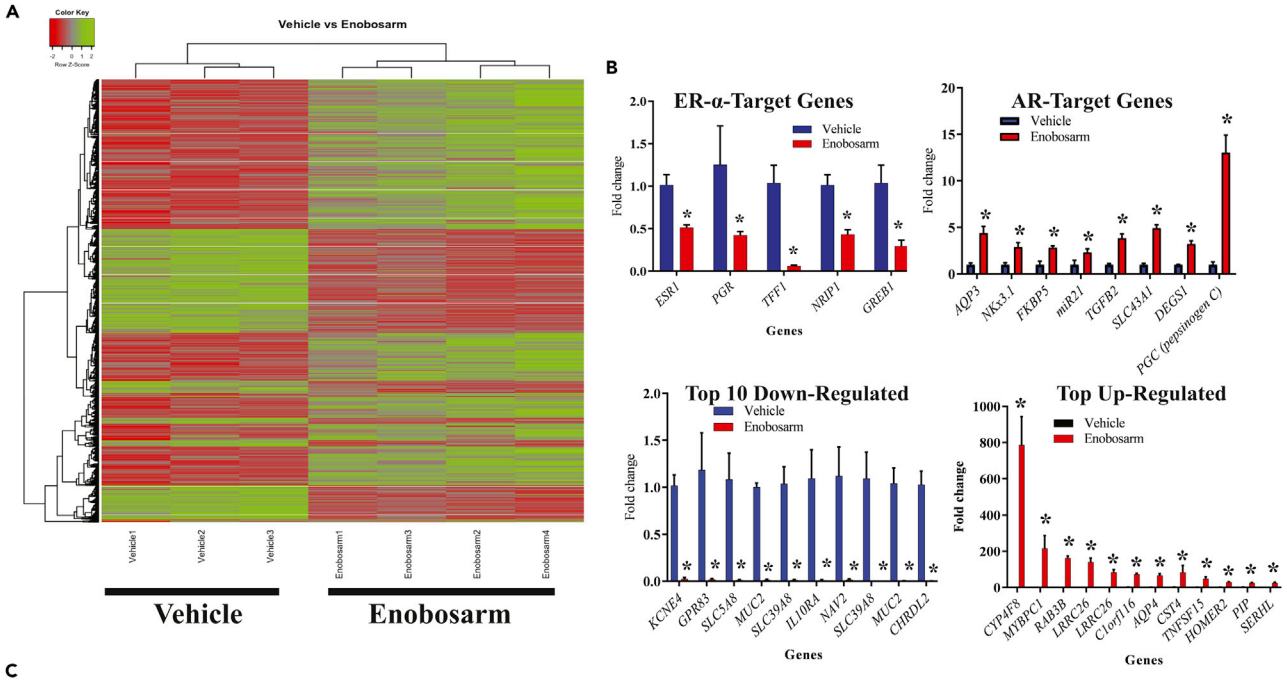

C

Canonical pathway	P-Value	Upstream regulator	P-Value	Diseases	P-Value
Glutamyl cycle	4.45E-04	ESR1	6.66E-11	Mammary tumor	1.02E-12
Tocopherol degradation	1.92E-03	NUPR1	1.78E-07	Breast cancer	1.65E-12
Glutathione-detox	2.13E-03	AR	2.83E-07	Breast/ovarian cancer	4.09E-10
Aryl H receptor signal	2.43E-03	E2F3	3.26E-07	Carcinoma of breast	2.31E-08
Unfold protein response	2.76E-03	CTR9	5.67E-07	Bening neoplasm	1.96E-06

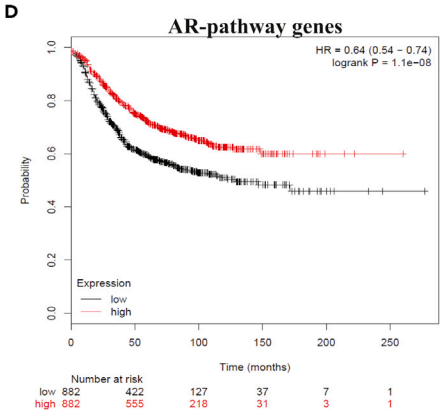

Figure 2. Gene Expression Study in HCI-13 PDX Indicates Inhibition of ER Pathway by an AR Agonist

(A–C) RNA was isolated from HCI-13 PDX xenografts treated with vehicle or enobosarm (Figure 1D) and microarray was performed (n = 3-4/group). Genes that were different in enobosarm-treated group ($q < 0.05$) are represented in the heatmap (A). Representative ER- and AR-target genes and the most up- and down-regulated genes are shown in panel (B). Canonical pathway, upstream regulators, and diseases represented by the enriched genes obtained from Ingenuity Pathway Analysis (IPA) are shown in panel (C).

(D) Genes enriched in the AR pathway were fed into TCGA database and Kaplan-Meier survival plots were created. * = $q < 0.05$. ER, estrogen receptor; AR, androgen receptor; PDX, patient-derived xenograft.

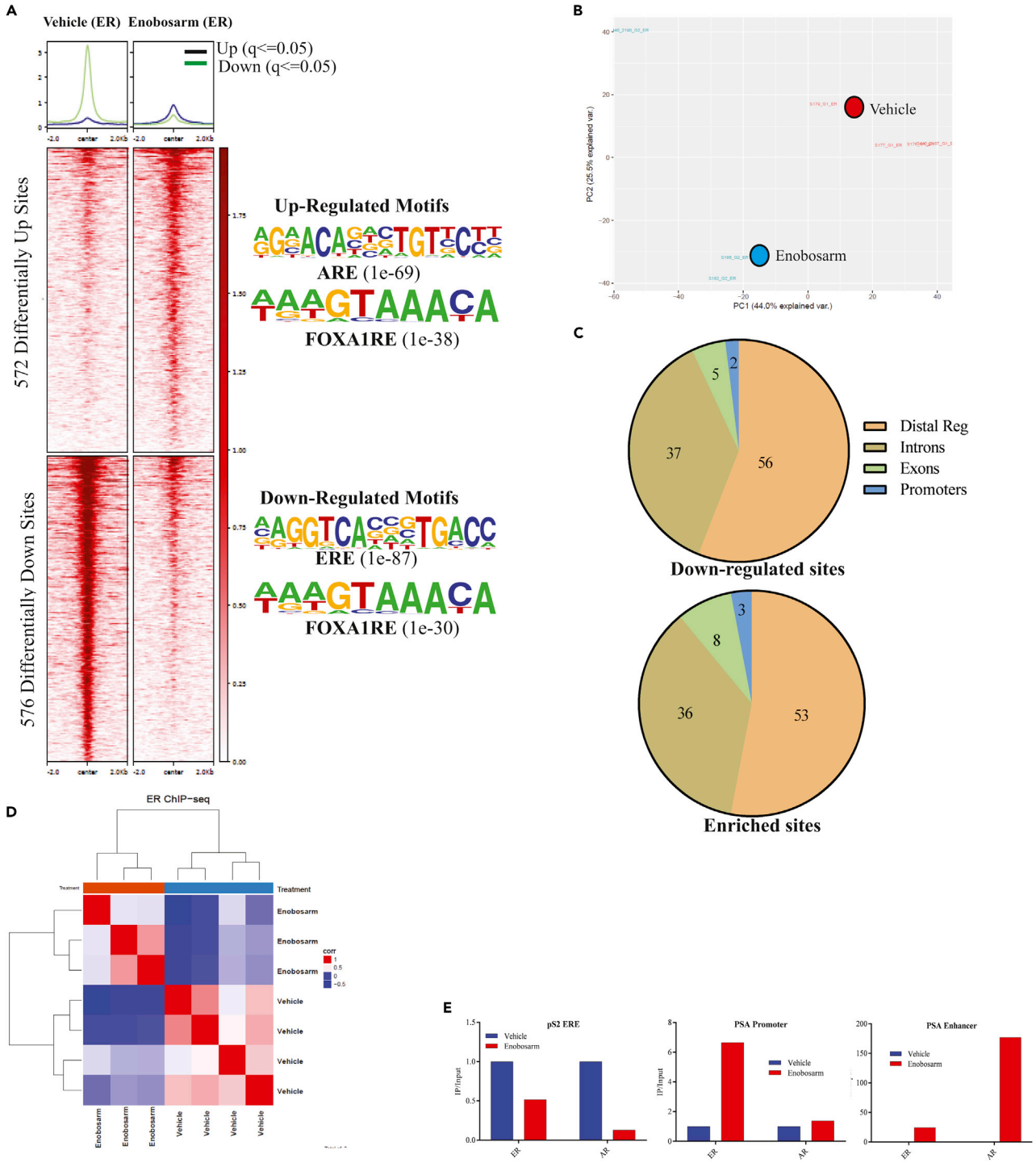

Figure 3. ChIP-sequencing Shows Reprogramming of ER Binding after Enobosarm Treatment

(A) Chromatin immunoprecipitation (ChIP) assay was performed for ER in tumors treated with vehicle (n = 4) or 10 mg/kg/day enobosarm (n = 3) (tumors from animals shown in Figure 1D). Next-generation sequencing was performed to determine the genome-wide binding of ER to the DNA. Heatmap of significantly different peaks (q < 0.05) is shown as average of the individual tumor samples. The top enriched motifs are shown to the right of the heatmap.

(B) Principal Component Analysis (PCA) plot of vehicle- and enobosarm-treated samples that corresponds to ER-ChIP peaks is shown.

(C) Pie charts showing the distribution of ER enrichment in enobosarm-treated HCI-13 samples.

Figure 3. *Continued*

(D) Unsupervised hierarchical clustering.

(E) ChIP assay was performed with ER antibody in HCI-13 specimens treated with vehicle or enobosarm and, real-time PCR was performed with the primers and TaqMan probe to the specified regions. AR, androgen receptor; ER, estrogen receptor; ChIP, chromatin immunoprecipitation; ARE, androgen response elements; ERE, estrogen response element; FOXA1RE, Forkhead box A1 response element.

individual samples, an indication that enobosarm modified the DNA-binding pattern of ER in HCI-13. The motifs that were enriched by the ER represent androgen response element (ARE) and FOXA1 response elements (FOXA1RE), whereas the regions that were depleted of ER represent estrogen response element (ERE) and FOXA1RE (Figure 3A right). Although the DNA regions depleted of ER by enobosarm favor the inhibition of the ER-target gene expression pattern, the enrichment of ER at AREs is surprising and has not been previously reported. Figure S5 shows representative regions enriched by and depleted of ER. Figure S6A shows the heatmap of individual tumor specimens. Variability between individual samples can be attributed to the inherent variability between xenograft specimens. Repeating the studies in a cell line model under controlled conditions might provide a robust redistribution outcome.

Between 50% and 60% of the ER-enriched and depleted sites were mapped to distal regulatory regions, whereas only around 2%–3% of the sites were mapped to promoter regions (Figure 3C). Interestingly, although the intron and exon binding percentage match with previous reports, the proportion of ER bound to promoters and distal regulatory elements are distinct from that observed in response to estrogens or with a constitutively active ER (Jeselsohn et al., 2018). Other studies have indicated that the ER cistrome comprises about 30%–40% distal regulatory regions and 7%–22% proximal promoter regions, whereas AR-regulated ER cistrome in this study comprises of 50%–60% and 2%–3% of these regions, respectively. ER binding to pS2 ERE, PSA (KLK3) promoter ARE, and PSA enhancer ARE was validated by ChIP real-time PCR (Figure 3E).

It was interesting to observe that an AR agonist such as enobosarm reprogrammed ER cistrome by depleting EREs of ER and enriching the AREs with ER. It is important to recognize that as enobosarm neither binds to ER nor alters ER activity (Kearbey et al., 2007; Narayanan et al., 2008); its effect on ER cistrome is mediated by activating AR. It is likely that ER is following AR or FOXA1 toward the respective response elements. We performed ChIP-Seq for AR in HCI-13 PDX treated with vehicle (n = 4) or enobosarm (n = 3). Enobosarm significantly enriched 5,156 sites, and no binding was observed in the absence of enobosarm (Figure 4A). As expected, the individual samples were distinctly positioned in the PCA plot (Figure 4B), and the motifs enriched by AR represent AREs and FOXA1RE (Figure 4A right). Figure S6B shows the heatmap of individual tumor specimens. The unsupervised hierarchical clustering shown in Figure 4C distinctly clustered the vehicle- and the enobosarm-treated samples.

Mapping the genomic regions bound by AR in HCI-13 indicates that genomic distribution is consistent with that of previously mapped region in LNCaP prostate cancer cells (Figure 4D) (Toropainen et al., 2016). We determined the overlap between ER and AR at statistically enriched sites to be 385 sites, which represent a remarkable 67% of the gained ER sites. AR alone occupies 4,777 out of 5,156 enriched sites, whereas ER alone occupies only 188 out of 572 ER-enriched sites (Figure 4E). This shows that new ER binding in the presence of an AR agonist is highly dependent on the AR occupancy. This warrants further exploration of a potential association between the two proteins on the ARE.

To determine if the AR cistrome in HCI-13 (where an agonist was growth inhibitory) in response to an agonist overlaps with AR cistrome in different models, a database search was performed. Most, if not all, of the AR cistromes found in the database search were identified in prostate cancer models. Table S3 shows a significant overlap between AR cistrome in HCI-13 and the AR cistromes in the database (TArbs = Tumor AR-binding sites (Pomerantz et al., 2015)).

Enobosarm Reprograms the FOXA1 Cistrome

It is interesting to observe that FOXA1RE motifs are represented in both enriched and depleted ER cistrome in response to enobosarm. Enrichment of FOXA1RE in the AR cistrome is not surprising, as previous studies have shown that the ligand-activated ER and AR bind to cis elements with FOXA1 binding adjacent to the ER and AR (Carroll et al., 2005; Zhao et al., 2016). Previous studies have also shown that FOXA1 binding is required for ER and AR to interact with the DNA at many genomic loci and that knockdown of FOXA1

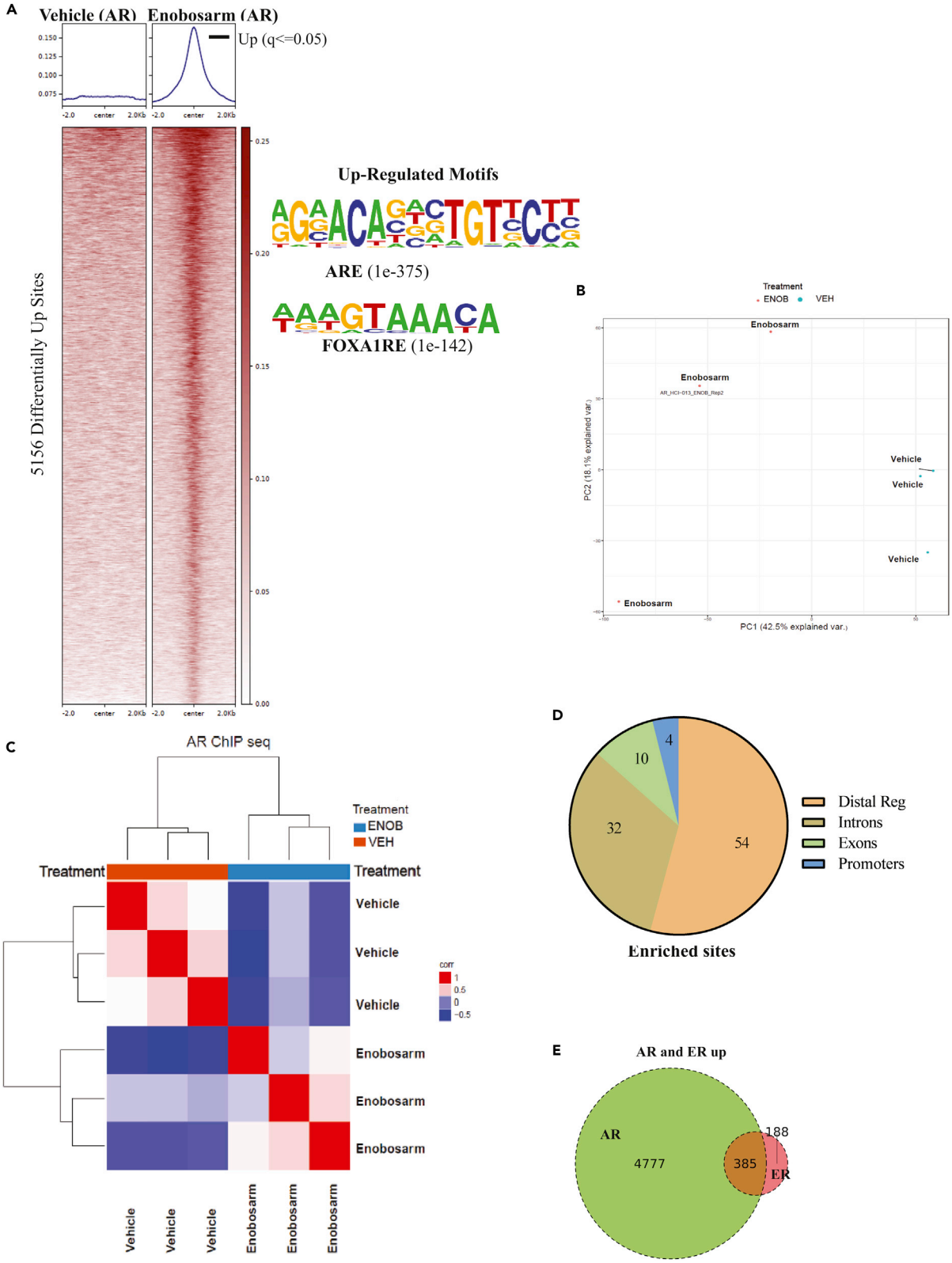
A
Vehicle (AR)
Enobosarm (AR)
Up (q<=0.05)
5156 Differentially Up Sites
Up-Regulated Motifs
ARE (1e-375)
FOXA1RE (1e-142)
B
Treatment
ENOB
VEH
Enobosarm
Vehicle
PC2 (18.1% explained var.)
PC1 (42.5% explained var.)
C
AR ChIP seq
Treatment
ENOB
VEH
Vehicle
Enobosarm
corr
D
Distal Reg
Introns
Exons
Promoters
Enriched sites
E
AR and ER up
AR
ER
4777
385
188

Figure 4. ChIP-sequencing Shows Rearrangement Binding of AR after Enobosarm Treatment

(A) Chromatin immunoprecipitation (ChIP) assay was performed for AR in tumors treated with vehicle (n = 4) or 10 mg/kg/day enobosarm (n = 3) (tumors from animals shown in Figure 1D). Next-generation sequencing was performed to determine the genome-wide binding of AR to the DNA. Heatmap of significantly different peaks ($q < 0.05$) is shown as average of the individual tumor samples. The top enriched and depleted motifs are shown to the right of the heatmap.

(B) Principal Component Analysis (PCA) plot of vehicle- and enobosarm-treated samples that corresponds to AR-ChIP peaks is shown.

(C) Unsupervised hierarchical clustering.

(D) Pie charts showing the distribution of AR enrichment in enobosarm-treated HCI-13 samples.

(E) AR and ER co-occupied sites represented as Venn diagram. AR, androgen receptor; ChIP, chromatin immunoprecipitation; ARE, androgen response elements; FOXA1RE, Forkhead box A1 response element.

reduces the association of ER and AR with chromatin (Carroll et al., 2005; Zhao et al., 2016). These results suggest that FOXA1 binding to DNA is an important event required for the AR and ER to function as transcription factors. Considering that FOXA1 is a critical pioneering transcription factor, we evaluated its interaction with DNA in the presence of vehicle and enobosarm treatment in HCI-13 PDX. Although FOXA1 is enriched in 4,946 DNA regions, it is depleted in 840 regions with a total of 5,786 DNA regions statistically altered in enobosarm-treated samples compared with the vehicle-treated samples (Figure 5A). Figure S6C shows the heatmap of individual tumor specimens. The PCA plot and hierarchical clustering distinctly segregates the samples belonging to the individual groups, suggesting that enobosarm clearly modifies FOXA1-chromatin interaction (Figures 5B and 5C). Enriched FOXA1 cistrome motifs represent ARE and FOXA1RE, whereas the depleted cistrome motifs represent ERE and FOXA1RE (Figure 5A right). This is consistent with the ER and AR ChIP-seq results. FOXA1 genomic binding regions are similar to that of ER and AR DNA binding regions and are consistent with earlier publications (Figure 5D). Out of the 4,946 gained FOXA1 sites, 2007 (40.6%) overlap with the gained AR-binding sites (Figure 5E). These results suggest a significant overlap between the gained AR and FOXA1 binding. Representative peaks for AR and FOXA1 are presented in Figure S7. Strikingly, out of the 840 sites with reduced FOXA1 binding, 474 overlap with lost ER-binding sites (83% of total ER sites and 56% of total FOX sites) (Figure 5E).

The above results were replotted to address whether the AR and FOXA1 were occupied or depleted from the ER-enriched or depleted sites in the presence of enobosarm (Figure S8A). Interestingly, ER enrichment is matched by the AR and FOXA1 enrichment, suggesting that all three transcription factors occupy the same sites. Similar to the enriched sites, ER-depleted sites were also depleted of FOXA1 binding (Figure S8A).

AR Agonist Inhibits ER-target Gene and ER-DNA Binding in HCI-7 Xenografts

Considering the impact on ER function observed in the presence of an AR agonist in ER-positive breast cancer PDX HCI-13, we performed experiments to confirm the gene expression and DNA occupancy results in a different ER-positive breast cancer model. RNA from HCI-7 tumors shown in Figure 1C was isolated and expression of ER and AR-target genes was measured by real-time PCR. Consistent with the HCI-13 PDX results, enobosarm increased the expression of AR-target gene *FKBP5* and significantly reduced the expression of ER-target genes *TFF1 (pS2)* and *PGR (PR)* (Figure 6A).

We further evaluated the DNA binding efficiency of ER in the presence of enobosarm in HCI-7 PDX tumor samples by ChIP-real time PCR (Figure 6B). ER occupancy on the *pS2* promoter in HCI-7 PDX was inhibited by enobosarm (Figure 6B). These results are consistent with the results observed in HCI-13 and suggest that these results are not model dependent.

Enobosarm Has No Effect on an AR-positive ER-negative Breast Cancer PDX

The results in ER-positive models indicate that the tumor suppressive function of AR is through indirect ER-inhibitory properties. If this is true, AR agonists should have no effect on ER-negative breast cancers. AR-positive ER-negative breast cancer HCI-9 tumor fragments were implanted under the mammary fat pad of NSG mice. Once the tumors grew to 100–200 mm^3, the animals were randomized and treated orally with vehicle or enobosarm. Enobosarm did not alter the tumor growth, indicating that the AR agonist was not effective in HCI-9 PDX that does not express ER (Figure 7A). This result was confirmed with another AR-positive TNBC PDX (data not shown). Enobosarm treatment increased the AR protein expression, indicating that it functioned as an agonist in this tumor model and the drug was delivered to the tumors (Figure 7B). The results of immunohistochemistry indicate that the tumors have minimal mouse stromal cells and the tumors predominantly comprised of epithelial cells with a ratio of 86:14% epithelial: stromal cells

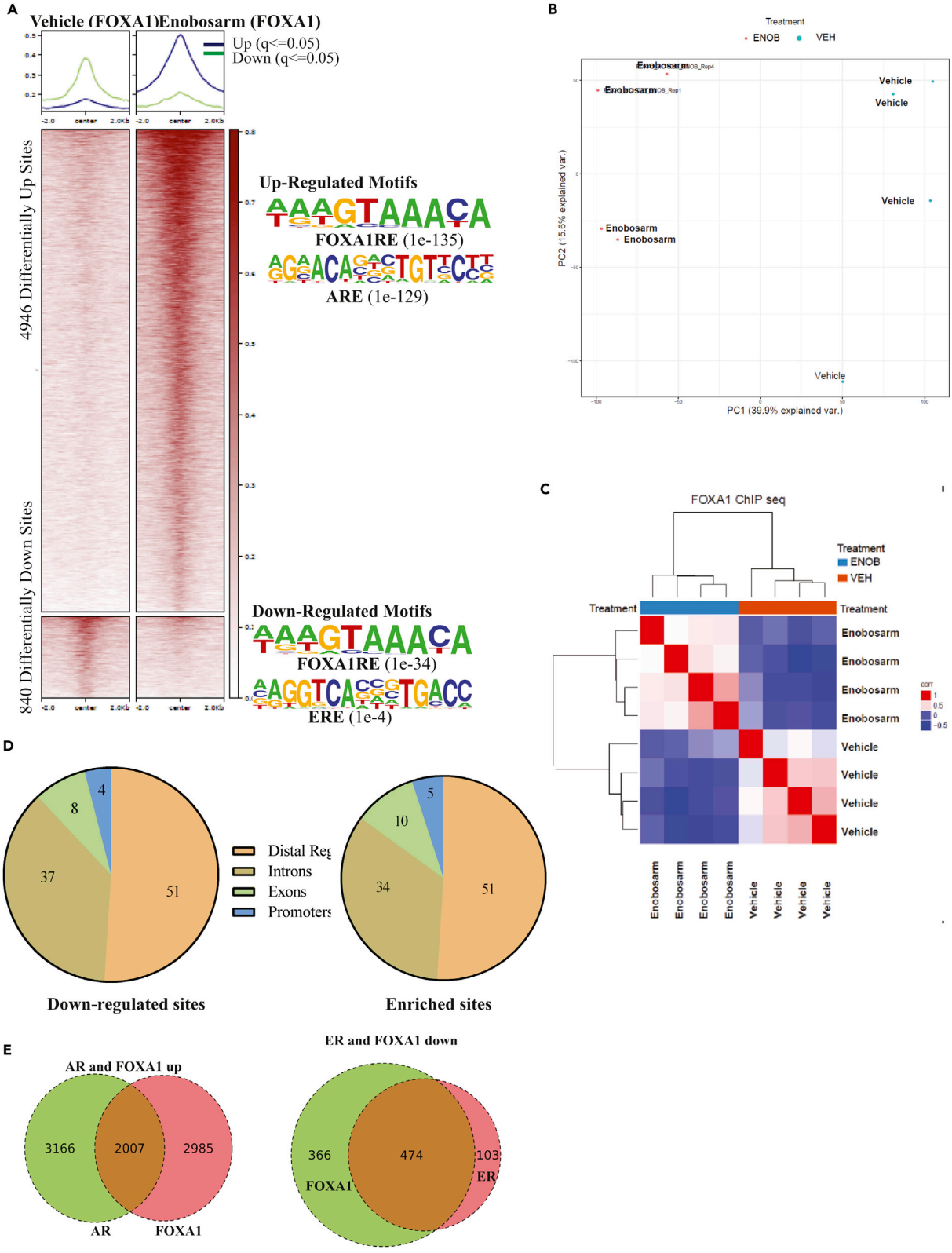
A
Vehicle (FOXA1)Enobosarm (FOXA1)
Up (q<=0.05)
Down (q<=0.05)
4946 Differentially Up Sites
840 Differentially Down Sites
Up-Regulated Motifs
FOXA1RE (1e-135)
ARE (1e-129)
Down-Regulated Motifs
FOXA1RE (1e-34)
ERE (1e-4)
B
Treatment
ENOB
VEH
PC1 (39.9% explained var.)
PC2 (15.6% explained var.)
C
FOXA1 ChIP seq
Treatment
ENOB
VEH
D
Distal Reg
Introns
Exons
Promoters
Down-regulated sites
Enriched sites
E
AR and FOXA1 up
3166
2007
2985
AR
FOXA1
ER and FOXA1 down
366
474
FOXA1
ER

Figure 5. ChIP-sequencing Shows Reprogramming of FOXA1 Binding to the DNA after Enobosarm Treatment

(A) ChIP assay was performed for FOXA1 in tumors treated with vehicle (n = 4) or 10 mg/kg/day enobosarm (n = 4) (tumors from animals shown in Figure 1D). Next-generation sequencing was performed to determine the genome-wide binding of FOXA1 to the DNA. Heatmap of significantly different peaks ($q < 0.05$) is shown as average of the individual tumor samples. The top enriched and depleted motifs are shown to the right of the heatmap.

(B) Principal Component Analysis (PCA) plot of vehicle- and enobosarm-treated samples that corresponds to FOXA1-ChIP peaks is shown.

(C) Unsupervised hierarchical clustering.

(D) Pie charts showing the distribution of FOXA1 enrichment in enobosarm-treated HCI-13 samples.

(E) AR and FOXA1 and ER and FOXA1 co-occupied sites represented as Venn diagram. FOXA1, Forkhear box A1; ChIP, chromatin immunoprecipitation; ARE, androgen response elements; GRE, glucocorticoid response elements; FOXA1RE, Forkhead box A1 response element.

(Figures 7C and 7D). Also, enobosarm had no effect on Ki-67 levels in the tumors. To ensure that the AR is functional, we extracted RNA from the tumors and performed real-time PCR for AR-target genes. Enobosarm significantly increased the expression of all AR-target genes that were measured, indicating that the AR is functional and responds to an AR agonist (Figure 7E). Finally, we performed preliminary ChIP-Seq with vehicle- and enobosarm-treated HCI-9 tumors to determine if the sites occupied by AR in HCI-13 are also occupied by AR in HCI-9 (Figure S8B). Although the HCI-9 ChIP-Seq was not performed in replicates, the preliminary results show the overlapping AR cistrome in ER-negative and -positive breast cancers.

Collectively, these results suggest that the AR mediates its anti-proliferative effects by indirectly inhibiting the growth promoting function of ER.

Co-localization of AR and ER in Luminal B Breast Cancer Cells

In order to determine the nuclear reactivity of AR and ER and potential co-localization in breast cancer specimens, immunohistochemistry was performed in several luminal B breast cancer specimens. Because this subtype is the faster growing of the two luminal types, luminal B subtype was chosen over luminal A. Relatively abundant nuclear immunoreactivity of both AR and ER was detected in all the breast cancer cases examined in this study (Figure S9 representative images). In addition, several cases examined had moderate levels of cytoplasmic immunoreactivity for both markers. As levels of immunoreactivity of both markers exceeded 60% in all the cases examined, a relatively high percentage of carcinoma cells were immunohistochemically positive for both ER and AR. The patterns of immunolocalization were also similar between these two markers above. Overall, the number of carcinoma cells immunohistochemically positive for AR in any one case exceeded those which were positive for ER. However, the semi-quantitative analysis of immunohistochemistry did preclude us from being able to state conclusively that AR was expressed at greater levels than ERα. It was also possible to detect the cases in which AR immunoreactivity was weaker or absent while ER immunoreactivity present, although less frequent.

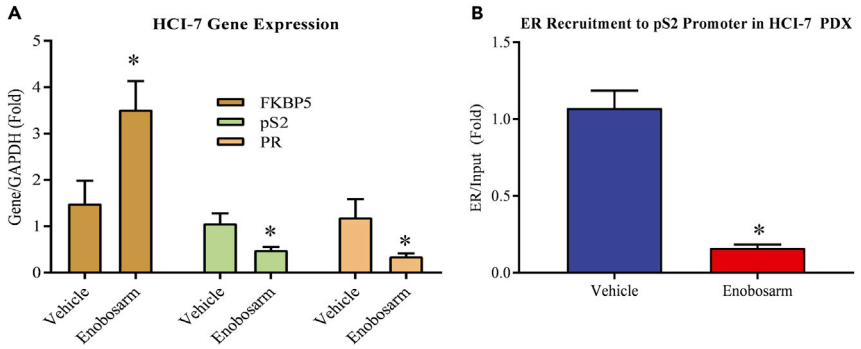

Figure 6. Enobosarm Effects on Gene Expression and ER Recruitment Are Reproducible in Different Models

(A) Enobosarm activates AR-target genes and inhibits ER-target genes in HCI-7 xenografts. RNA was extracted from vehicle- or enobosarm-treated HCI-7 tumor tissues (n = 4/group), and expression of the indicated genes was measured by real-time PCR.

(B) Enobosarm inhibits ER recruitment to pS2 promoter in HCI-7 tumors. HCI-7 tumors that were treated with vehicle or enobosarm (n = 3/group) were snap-frozen at the time of collection. Tumors were formalin fixed, homogenized, and ER immunoprecipitated with an ER antibody. Real-time PCR was performed for the pS2 promoter EREs. *$p < 0.05$.

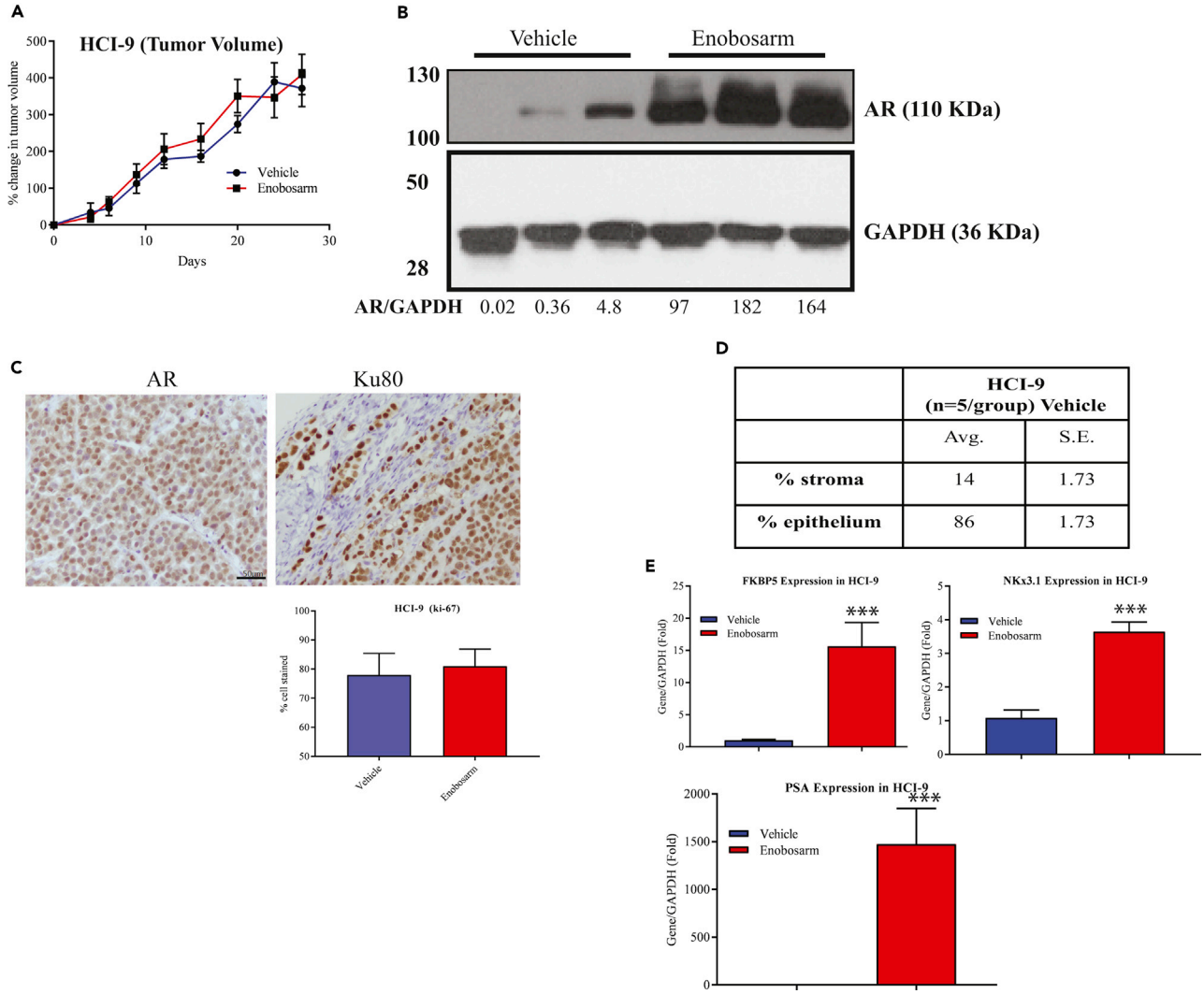

Figure 7. Enobosarm Does Not Inhibit Growth of an ER-negative AR-positive HCI-9 PDX

(A) AR-positive, but ER-negative, HCI-9 PDX was surgically implanted as 1 mm^3 fragments under the mammary fat pad in intact NSG mice (n = 8–10/group). Once the tumors reached 100–200 mm^3, the mice were randomized and treated with vehicle (DMSO:PEG-300 (15%:85%)) or enobosarm (10 mpk p.o.). Tumor volume was measured thrice weekly.

(B) AR Western blot was performed from the tumor specimens shown on the left. Densitometric quantification of the bands is provided at the bottom of the blot.

(C) HCI-9 tumors were formalin-fixed and immunostained with the indicated antibodies. Representative images of n = 4–5/group/stain are shown. Ki-67 staining was quantified and represented as bar graph (n = 5/group). Scale is provided in one of the images (50 μm).

(D) Table showing the percent of stromal and epithelial cells in the xenografts.

(E) Enobosarm increases AR-target genes. HCI-9 tumor fragments from vehicle- or enobosarm-treated samples (n = 4/group) were homogenized and RNA isolated. Expression of AR-target genes was measured by real-time PCR and normalized to GAPDH expression. Data are represented as fold change from vehicle-treated samples.

Protein-Pathway Activation Mapping Shows Inhibition of Oncogenic and Induction of Tumor-Suppressor Protein Phosphorylation by Enobosarm

To determine the effect of enobosarm on protein signaling, we performed RPPA-based analysis in HCI-13 tumors treated with vehicle or enobosarm to measure the phosphorylation and total levels of protein in key signaling pathways known to be involved in tumorigenesis and metastatic progression. Enobosarm inhibited the phosphorylation of various oncogenic proteins such as pERK, PKC ζ, RSK3, Ezrin, BCL2, ELF4G, and ER (Figure S10). Enobosarm also inhibited the expression of proliferation marker Ki67. Alternatively, enobosarm increased the phosphorylation of tumor suppressor proteins such as p53, p27, and

ACC. AR phosphorylation was also increased in enobosarm-treated samples. Enobosarm also increased the phosphorylation of STAT5, which could be a tumor suppressor or an oncogene depending on the context (Figure S10). These results demonstrate that activating the AR with an agonist promotes the alteration of appropriate pathways that facilitate tumor growth inhibition. These results were confirmed using Western blots for phospho Ser^{81} AR and phospho Ser^{118} ER (Figure S10 lower blots).

DISCUSSION

Although breast cancer was often successfully treated with steroidal androgens until the development of ER-targeted therapies, unwanted virilizing effects have limited their clinical use. SARMs that tissue-selectively activate the AR are currently being developed for multiple indications, including muscle wasting, osteoporosis, muscular dystrophy, breast cancer, and urinary incontinence. Enobosarm, which has been tested in the clinic (Crawford et al., 2016; Dobs et al., 2013), has demonstrated pharmacologic effects consistent with selective AR targeting. In clinical trials, enobosarm increased lean body mass by more than a kilogram and performance of various muscles (Dobs et al., 2013) and has not shown virilizing effects at the 3 mg dose. In addition, enobosarm treatment has demonstrated clinical benefit in women with ER-positive breast cancer who previously responded to hormonal therapies (San Antonio breast cancer symposium, 2015) (Overmoyer, 2015). Women who were extensively treated with ER-targeted therapies could be benefited by these secondary bone and muscle building effects of AR agonists such as the SARMs.

The results obtained in this study are encouraging. A tumor (HCI-13) that relapsed and continued to grow in the presence of a range of therapeutics was inhibited by AR agonists. This result and the result from *ex vivo* studies support the use of AR agonists even after the tumors relapse from other treatment options. The mutation represented in HCI-13, Y537S, is one of the common mutants found in the clinic (Katzenellenbogen et al., 2018).

The unique property of inhibiting the ER function by activating the AR demonstrates the complex interaction between various nuclear receptors and their associated proteins. The microarray results indicate that the inhibition of ER pathway by an AR agonist could provide greater benefit to patients in whom the oncogenic pathway is constitutively active. This beneficial effect is further enhanced by the increase in the phosphorylation of various tumor suppressors and inhibition of the phosphorylation of oncogenes.

The ChIP-Seq results suggest that the AR, ER, and FOXA1 colocalized in the presence of AR agonist and shift from ER cistrome to AR cistrome. As FOXA1 pioneering transcription factor is important for the function of both AR and ER and has overlapping binding sites with ARE and ERE (Carroll et al., 2005; Wang et al., 2007), it is possible that the activated AR might sequester FOXA1 from the FOXA1REs adjacent to the EREs to open up the nucleosome and facilitate its binding to ARE. Based on these results, we propose a model (Figure 8) wherein the absence of androgen or estrogen, the DNA is in a condensed conformation where the EREs, AREs, and FOXA1REs are unbound. FOXA1 occupies FOXA1REs in the absence of estrogens or androgens, and upon estradiol exposure, FOXA1 opens the chromatin and binds to its response elements adjacent to the EREs. This facilitates the ER to bind to its response elements and promote the transcription of the target genes. While this is ongoing, AR is not bound to AREs. However, when an AR agonist binds to the AR, it changes conformation and proceeds to bind to AREs that may or may not be near pre-existing FOXA1 sites. Strikingly, ER binding is significantly reduced at its original sites and is significantly gained at new sites highly overlapping with the AR gained sites. The mechanism for this reprogramming is not clear at the molecular level, but likely involves FOXA1, which is lost at many of the original ER-binding sites and gained at many of the new AR-binding sites and so might be due to squelching. Future studies will need to determine whether the ER's interaction with AREs is due to a complex formed with AR or through FOXA1. The stoichiometry and interaction sites of ER and AR in these AR agonist-induced complexes also remains uncertain as is the role that squelching of FOXA1 or other co-factors may play in this nuclear hormone receptor reprogramming.

Clinical trial results with enobosarm (presented in San Antonio Breast Cancer Symposium in 2015 and 2016) already demonstrated a favorable outcome in patients who have relapsed from hormonal therapies. Twenty-two patients with breast cancer were treated with 9 mg of enobosarm. Of the 17 AR-positive patients, 35.3% achieved clinical benefit after six months of treatment with 9 mg enobosarm administered once daily. These results will be published in the future.

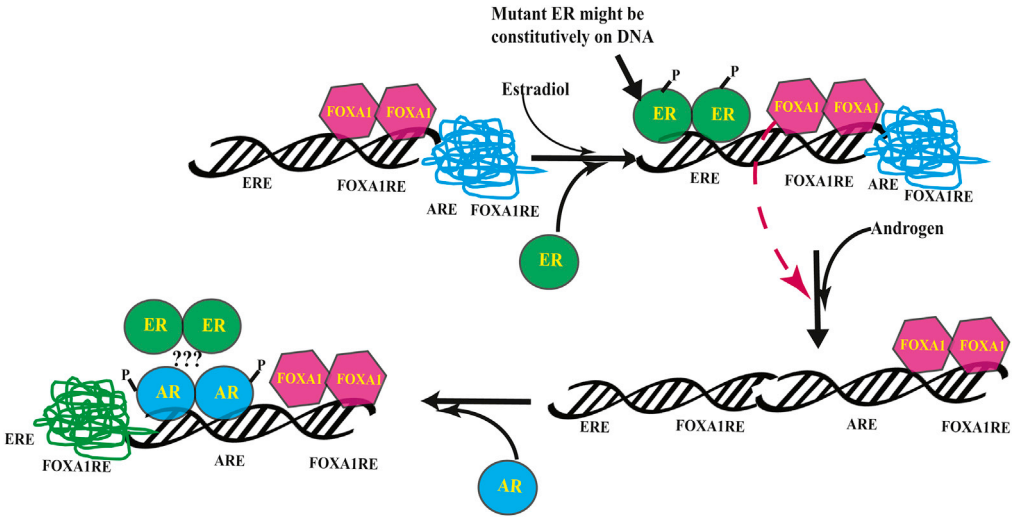

Figure 8. Model Depicting the Regulation of ER Function by AR Ligands

The model shows the redistribution of transcription factors AR, ER, and FOXA1 when AR is activated by an agonist. AR, androgen receptor; ER, estrogen receptor; ARE, androgen response element; ERE, estrogen response element; FOXA1RE, FOXA1 response element.

Overall, these mechanism-based preclinical and translational studies support the use of an AR agonist to treat refractory hormone receptor-positive breast cancer. Various advantages that an AR agonist will confer include tumor growth inhibition, muscle mass increase, increase in bone mass, better cognition, improvement in sexual function, and reduction in the incidence of urinary incontinence (Ho et al., 2004; Kearbey et al., 2009; Ponnusamy et al., 2017a, 2017b). Tissue-selective AR agonism might offer an alternative hormonal approach for hormone receptor-positive breast cancers.

Limitations of the Study

Although the results support the mechanism of action and the tumor suppressive role of AR in ER-positive breast cancer, we recognize several limitations in this work. First, the ChIP-Seq and mechanistic studies were conducted in one PDX and with one SARM. Future studies need to be conducted in multiple ER-positive PDXs using different AR agonists to validate the findings. Secondly, because the concept was tested in one wild-type ER-positive and one mutant ER-positive PDX, the results need to be validated in additional PDXs of each type. Other ER-LBD mutants need to be included in such studies to deduce a comprehensive conclusion. Finally, the role of AR antagonists needs to be evaluated in detail using PDX models to understand why under certain conditions, especially in cellular models, they inhibit ER-positive breast cancer growth.

METHODS

All methods can be found in the accompanying Transparent Methods supplemental file.

DATA AND CODE AVAILABILITY

Accession number for the sequencing data from public deposition is GSE128018. Microarray data was deposited in GEO and the accession number is GSE126318.

SUPPLEMENTAL INFORMATION

Supplemental Information can be found online at https://doi.org/10.1016/j.isci.2019.10.038.

ACKNOWLEDGMENTS

The authors thank UTHSC molecular resource center for their help with microarray experiments. The authors thank Dr. Dejian Ma, department of pharmaceutical sciences, UTHSC Mass Spectrometry core for his help with the LC-MS/MS measurement of drug concentration. The studies were partially funded by a research grant from GTx, Inc.

AUTHOR CONTRIBUTIONS

SP, SA, and TT performed all animal experiments, *ex vivo* sponge cultures, RNA isolation and gene expression studies, and ChIP-PCR assay. RN conceived and designed the experiments and managed the overall project. LSS managed the clinical aspects of the project with the help of BG, MDF, FEP, MPB, RO, and REF. HS and KMM designed the IHC part, which were executed by FG. HL and MB planned and managed the ChIP-Seq experiments, whereas AFT and PKR performed the experiments. XQ, YX, and DLJ provided bioinformatics and statistical support. EFP planned the RPPA studies, whereas MP performed the experiments.

DECLARATION OF INTERESTS

RN is a consultant to GTx, Inc., Memphis. This role has not influenced the conduct of experiments and the interpretation of results.

Received: September 10, 2019
Revised: October 8, 2019
Accepted: October 18, 2019
Published: November 22, 2019

REFERENCES

Adair, F.E., and Herrmann, J.B. (1946). The use of testosterone propionate in the treatment of advanced carcinoma of the breast. Ann. Surg. *123*, 1023–1035.

Aleskandarany, M.A., Abduljabbar, R., Ashankyty, I., Elmouna, A., Jerjees, D., Ali, S., Buluwela, L., Diez-Rodriguez, M., Caldas, C., Green, A.R., et al. (2016). Prognostic significance of androgen receptor expression in invasive breast cancer: transcriptomic and protein expression analysis. Breast Cancer Res. Treat. *159*, 215–227.

Allard, J., Li, K., Lopez, X.M., Blanchard, S., Barbot, P., Rorive, S., Decaestecker, C., Pochet, R., Bohl, D., Lepore, A.C., et al. (2014). Immunohistochemical toolkit for tracking and quantifying xenotransplanted human stem cells. Regen. Med. *9*, 437–452.

Andersen, J., and Poulsen, H.S. (1989). Immunohistochemical estrogen receptor determination in paraffin-embedded tissue. Prediction of response to hormonal treatment in advanced breast cancer. Cancer *64*, 1901–1908.

Balbas, M.D., Evans, M.J., Hosfield, D.J., Wongvipat, J., Arora, V.K., Watson, P.A., Chen, Y., Greene, G.L., Shen, Y., and Sawyers, C.L. (2013). Overcoming mutation-based resistance to antiandrogens with rational drug design. Elife *2*, e00499.

Barton, V.N., Christenson, J.L., Gordon, M.A., Greene, L.I., Rogers, T.J., Butterfield, K., Babbs, B., Spoelstra, N.S., D'Amato, N.C., Elias, A., et al. (2017). Androgen receptor supports an anchorage-independent, cancer stem cell-like population in triple-negative breast cancer. Cancer Res. *77*, 3455–3466.

Bray, F., Ferlay, J., Soerjomataram, I., Siegel, R.L., Torre, L.A., and Jemal, A. (2018). Global cancer statistics 2018: GLOBOCAN estimates of incidence and mortality worldwide for 36 cancers in 185 countries. CA Cancer J. Clin. *68*, 394–424.

Bronte, G., Rocca, A., Ravaioli, S., Puccetti, M., Tumedei, M.M., Scarpi, E., Andreis, D., Maltoni, R., Sarti, S., Cecconetto, L., et al. (2018). Androgen receptor in advanced breast cancer: is it useful to predict the efficacy of anti-estrogen therapy? BMC Cancer *18*, 348.

Cao, L., Xiang, G., Liu, F., Xu, C., Liu, J., Meng, Q., Lyu, S., Wang, S., and Niu, Y. (2019). A high AR: ERalpha or PDEF: ERalpha ratio predicts a suboptimal response to tamoxifen therapy in ERalpha-positive breast cancer. Cancer Chemother. Pharmacol. *84*, 609–620.

Carroll, J.S., Liu, X.S., Brodsky, A.S., Li, W., Meyer, C.A., Szary, A.J., Eeckhoute, J., Shao, W., Hestermann, E.V., Geistlinger, T.R., et al. (2005). Chromosome-wide mapping of estrogen receptor binding reveals long-range regulation requiring the forkhead protein FoxA1. Cell *122*, 33–43.

Chandarlapaty, S., Chen, D., He, W., Sung, P., Samoila, A., You, D., Bhatt, T., Patel, P., Voi, M., Gnant, M., et al. (2016). Prevalence of ESR1 mutations in cell-free DNA and outcomes in metastatic breast cancer: a secondary analysis of the BOLERO-2 clinical trial. JAMA Oncol. *2*, 1310–1315.

Ciupek, A., Rechoum, Y., Gu, G., Gelsomino, L., Beyer, A.R., Brusco, L., Covington, K.R., Tsimelzon, A., and Fuqua, S.A. (2015). Androgen receptor promotes tamoxifen agonist activity by activation of EGFR in ERalpha-positive breast cancer. Breast Cancer Res. Treat. *154*, 225–237.

Cochrane, D.R., Bernales, S., Jacobsen, B.M., Cittelly, D.M., Howe, E.N., D'Amato, N.C., Spoelstra, N.S., Edgerton, S.M., Jean, A., et al. (2014). Role of the androgen receptor in breast cancer and preclinical analysis of enzalutamide. Breast Cancer Res. *16*, R7.

Collins, L.C., Cole, K.S., Marotti, J.D., Hu, R., Schnitt, S.J., and Tamimi, R.M. (2011). Androgen receptor expression in breast cancer in relation to molecular phenotype: results from the Nurses' Health Study. Mod. Pathol. *24*, 924–931.

Crawford, J., Prado, C.M., Johnston, M.A., Gralla, R.J., Taylor, R.P., Hancock, M.L., and Dalton, J.T. (2016). Study design and rationale for the phase 3 clinical development program of enobosarm, a selective androgen receptor modulator, for the prevention and treatment of muscle wasting in cancer patients (POWER trials). Curr. Oncol. Rep. *18*, 37.

Creevey, L., Bleach, R., Madden, S.F., Toomey, S., Bane, F.T., Vareslija, D., Hill, A.D., Young, L.S., and McIlroy, M. (2019). Altered steroid milieu in AI resistant breast cancer facilitates AR mediated gene expression associated with poor response to therapy. Mol. Cancer Ther. *18*, 1731–1743.

D'Amato, N.C., Gordon, M.A., Babbs, B., Spoelstra, N.S., Carson Butterfield, K.T., Torkko, K.C., Phan, V.T., Barton, V.N., Rogers, T.J., Sartorius, C.A., et al. (2016). Cooperative dynamics of AR and ER activity in breast cancer. Mol. Cancer Res. *14*, 1054–1067.

Dalton, J.T., Barnette, K.G., Bohl, C.E., Hancock, M.L., Rodriguez, D., Dodson, S.T., Morton, R.A., and Steiner, M.S. (2011). The selective androgen receptor modulator GTx-024 (enobosarm) improves lean body mass and physical function in healthy elderly men and postmenopausal women: results of a double-blind, placebo-controlled phase II trial. J. Cachexia Sarcopenia Muscle *2*, 153–161.

Dalton, J.T., Mukherjee, A., Zhu, Z., Kirkovsky, L., and Miller, D.D. (1998). Discovery of nonsteroidal androgens. Biochem. Biophys. Res. Commun. *244*, 1–4.

Danforth, K.N., Eliassen, A.H., Tworoger, S.S., Missmer, S.A., Barbieri, R.L., Rosner, B.A., Colditz, G.A., and Hankinson, S.E. (2010). The association of plasma androgen levels with breast, ovarian and endometrial cancer risk factors among postmenopausal women. Int. J. Cancer *126*, 199–207.

De Amicis, F., Thirugnansampanthan, J., Cui, Y., Selever, J., Beyer, A., Parra, I., Weigel, N.L., Herynk, M.H., Tsimelzon, A., Lewis, M.T., et al. (2010). Androgen receptor overexpression induces tamoxifen resistance in human breast cancer cells. Breast Cancer Res. Treat. *121*, 1–11.

DeRose, Y.S., Wang, G., Lin, Y.C., Bernard, P.S., Buys, S.S., Ebbert, M.T., Factor, R., Matsen, C., Milash, B.A., Nelson, E., et al. (2011). Tumor grafts derived from women with breast cancer authentically reflect tumor pathology, growth, metastasis and disease outcomes. Nat. Med. *17*, 1514–1520.

Dobs, A.S., Boccia, R.V., Croot, C.C., Gabrail, N.Y., Dalton, J.T., Hancock, M.L., Johnston, M.A., and Steiner, M.S. (2013). Effects of enobosarm on muscle wasting and physical function in patients with cancer: a double-blind, randomised controlled phase 2 trial. Lancet Oncol. *14*, 335–345.

Early Breast Cancer Trialists' Collaborative Group, Dowsett, M., Forbes, J.F., Bradley, R., Ingle, J., Aihara, T., Bliss, J., Boccardo, F., Coates, A., Coombes, R.C., et al. (2015). Aromatase inhibitors versus tamoxifen in early breast cancer: patient-level meta-analysis of the randomised trials. Lancet *386*, 1341–1352.

Eastell, R., Adams, J.E., Coleman, R.E., Howell, A., Hannon, R.A., Cuzick, J., Mackey, J.R., Beckmann, M.W., and Clack, G. (2008). Effect of anastrozole on bone mineral density: 5-year results from the anastrozole, tamoxifen, alone or in combination trial 18233230. J. Clin. Oncol. *26*, 1051–1057.

Fuqua, S.A., Chamness, G.C., and McGuire, W.L. (1993). Estrogen receptor mutations in breast cancer. J. Cell Biochem. *51*, 135–139.

Garay, J.P., and Park, B.H. (2012). Androgen receptor as a targeted therapy for breast cancer. Am. J. Cancer Res. *2*, 434–445.

Gordan, G.S., Graham, W.P., 3rd, Goldman, L., Papac, R., Sheline, G.E., Vaeth, J., and Witt, J. (1963). Hormonal treatment of disseminated cancer of the female breast. Calif. Med. *98*, 189–194.

Guo, S., Zhang, C., Bratton, M., Mottamal, M., Liu, J., Ma, P., Zheng, S., Zhong, Q., Yang, L., Wiese, T.E., et al. (2018). ZB716, a steroidal selective estrogen receptor degrader (SERD), is orally efficacious in blocking tumor growth in mouse xenograft models. Oncotarget *9*, 6924–6937.

Hara, T., Miyazaki, J., Araki, H., Yamaoka, M., Kanzaki, N., Kusaka, M., and Miyamoto, M. (2003). Novel mutations of androgen receptor: a possible mechanism of bicalutamide withdrawal syndrome. Cancer Res. *63*, 149–153.

Heise, E., and Gorlich, M. (1982). Estradiol receptor activity in human breast cancer, disease free interval and survival time. Anticancer Res. *2*, 33–36.

Ho, M.H., Bhatia, N.N., and Bhasin, S. (2004). Anabolic effects of androgens on muscles of female pelvic floor and lower urinary tract. Curr. Opin. Obstet. Gynecol. *16*, 405–409.

https://finance.yahoo.com/news/gtx-announces-top-line-results-120000738.html. https://finance.yahoo.com/news/gtx-announces-top-line-results-120000738.html.

Hu, R., Dawood, S., Holmes, M.D., Collins, L.C., Schnitt, S.J., Cole, K., Marotti, J.D., Hankinson, S.E., Colditz, G.A., and Tamimi, R.M. (2011). Androgen receptor expression and breast cancer survival in postmenopausal women. Clin. Cancer Res. *17*, 1867–1874.

Jeselsohn, R., Bergholz, J.S., Pun, M., Cornwell, M., Liu, W., Nardone, A., Xiao, T., Li, W., Qiu, X., Buchwalter, G., et al. (2018). Allele-specific chromatin recruitment and therapeutic vulnerabilities of ESR1 activating mutations. Cancer Cell *33*, 173–186.e5.

Jin, Y., and Penning, T.M. (2001). Steroid 5alpha-reductases and 3alpha-hydroxysteroid dehydrogenases: key enzymes in androgen metabolism. Best Pract. Res. Clin. Endocrinol. Metab. *15*, 79–94.

Kaaks, R., Berrino, F., Key, T., Rinaldi, S., Dossus, L., Biessy, C., Secreto, G., Amiano, P., Bingham, S., Boeing, H., et al. (2005). Serum sex steroids in premenopausal women and breast cancer risk within the European Prospective Investigation into Cancer and Nutrition (EPIC). J. Natl. Cancer Inst. *97*, 755–765.

Kandouz, M., Lombet, A., Perrot, J.Y., Jacob, D., Carvajal, S., Kazem, A., Rostene, W., Therwath, A., and Gompel, A. (1999). Proapoptotic effects of antiestrogens, progestins and androgen in breast cancer cells. J. Steroid Biochem. Mol. Biol. *69*, 463–471.

Karnik, P.S., Kulkarni, S., Liu, X.P., Budd, G.T., and Bukowski, R.M. (1994). Estrogen receptor mutations in tamoxifen-resistant breast cancer. Cancer Res. *54*, 349–353.

Katzenellenbogen, J.A., Mayne, C.G., Katzenellenbogen, B.S., Greene, G.L., and Chandarlapaty, S. (2018). Structural underpinnings of oestrogen receptor mutations in endocrine therapy resistance. Nat. Rev. Cancer *18*, 377–388.

Kearbey, J.D., Gao, W., Fisher, S.J., Wu, D., Miller, D.D., and Dalton, J.T. (2009). Effects of selective androgen receptor modulator (SARM) treatment in osteopenic female rats. Pharm. Res. *26*, 2471–2477.

Kearbey, J.D., Gao, W., Narayanan, R., Fisher, S.J., Wu, D., Miller, D.D., and Dalton, J.T. (2007). Selective Androgen Receptor Modulator (SARM) treatment prevents bone loss and reduces body fat in ovariectomized rats. Pharm. Res. *24*, 328–335.

Kemppainen, J.A., Lane, M.V., Sar, M., and Wilson, E.M. (1992). Androgen receptor phosphorylation, turnover, nuclear transport, and transcriptional activation. Specificity for steroids and antihormones. J. Biol. Chem. *267*, 968–974.

Kennedy, B.J. (1958). Fluoxymesterone therapy in advanced breast cancer. N. Engl. J. Med. *259*, 673–675.

Liao, D.J., and Dickson, R.B. (2002). Roles of androgens in the development, growth, and carcinogenesis of the mammary gland. J. Steroid Biochem. Mol. Biol. *80*, 175–189.

Magnani, L., Frige, G., Gadaleta, R.M., Corleone, G., Fabris, S., Kempe, H., Verschure, P.J., Barozzi, I., Vircillo, V., Hong, S.P., et al. (2017). Acquired CYP19A1 amplification is an early specific mechanism of aromatase inhibitor resistance in ERalpha metastatic breast cancer. Nat. Genet. *49*, 444–450.

Maykel, J., Liu, J.H., Li, H., Shultz, L.D., Greiner, D.L., and Houghton, J. (2014). NOD-scidIl2rg (tm1Wjl) and NOD-Rag1 (null) Il2rg (tm1Wjl) : a model for stromal cell-tumor cell interaction for human colon cancer. Dig. Dis. Sci. *59*, 1169–1179.

Musgrove, E.A., and Sutherland, R.L. (2009). Biological determinants of endocrine resistance in breast cancer. Nat. Rev. Cancer *9*, 631–643.

Narayanan, R., Ahn, S., Cheney, M.D., Yepuru, M., Miller, D.D., Steiner, M.S., and Dalton, J.T. (2014). Selective androgen receptor modulators (SARMs) negatively regulate triple-negative breast cancer growth and epithelial:mesenchymal stem cell signaling. PLoS One *9*, e103202.

Narayanan, R., Coss, C.C., Yepuru, M., Kearbey, J.D., Miller, D.D., and Dalton, J.T. (2008). Steroidal androgens and nonsteroidal, tissue-selective androgen receptor modulator, S-22, regulate androgen receptor function through distinct genomic and nongenomic signaling pathways. Mol. Endocrinol. *22*, 2448–2465.

Narita, D., Raica, M., Suciu, C., Cimpean, A., and Anghel, A. (2006). Immunohistochemical expression of androgen receptor and prostate-specific antigen in breast cancer. Folia Histochem. Cytobiol. *44*, 165–172.

Neifeld, J.P., Lawrence, W., Jr., Brown, P.W., Banks, W.L., and Terz, J.J. (1982). Estrogen receptors in primary breast cancer. Arch. Surg. *117*, 753–757.

Niemeier, L.A., Dabbs, D.J., Beriwal, S., Striebel, J.M., and Bhargava, R. (2010). Androgen receptor in breast cancer: expression in estrogen receptor-positive tumors and in estrogen receptor-negative tumors with apocrine differentiation. Mod. Pathol. *23*, 205–212.

Oliveira, A.G., Coelho, P.H., Guedes, F.D., Mahecha, G.A., Hess, R.A., and Oliveira, C.A. (2007). 5alpha-Androstane-3beta,17beta-diol (3beta-diol), an estrogenic metabolite of 5alpha-dihydrotestosterone, is a potent modulator of estrogen receptor ERbeta expression in the ventral prostrate of adult rats. Steroids *72*, 914–922.

Overmoyer, B. (2015). Phase 2 open label, multinational, randomized, parallel design study investigating the efficacy and safety of GTx-024 on metastatic (MET) or locally advanced (LA) ER+/AR+ breast cancer (BC) in postmenopausal (PM) women. Paper presented at: San Antonio Breast Cancer Symposium OT2-01-06 (San Antonio).

Park, B.Y., Grisham, R.N., den Hollander, B., Thapi, D., Berman, T., de Stanchina, E., Zhou, Q., Iyer, G., Aghajanian, C., and Spriggs, D.R. (2016). Tumor inhibition by enzalutamide in a xenograft model of ovarian cancer. Cancer Invest. *34*, 517–520.

Perou, C.M., Sorlie, T., Eisen, M.B., van de Rijn, M., Jeffrey, S.S., Rees, C.A., Pollack, J.R., Ross, D.T., Johnsen, H., Akslen, L.A., et al. (2000). Molecular portraits of human breast tumours. Nature *406*, 747–752.

Pollock, J.A., Wardell, S.E., Parent, A.A., Stagg, D.B., Ellison, S.J., Alley, H.M., Chao, C.A., Lawrence, S.A., Stice, J.P., Spasojevic, I., et al. (2016). Inhibiting androgen receptor nuclear entry in castration-resistant prostate cancer. Nat. Chem. Biol. *12*, 795–801.

Pomerantz, M.M., Li, F., Takeda, D.Y., Lenci, R., Chonkar, A., Chabot, M., Cejas, P., Vazquez, F.,

Cook, J., Shivdasani, R.A., et al. (2015). The androgen receptor cistrome is extensively reprogrammed in human prostate tumorigenesis. Nat. Genet. *47*, 1346–1351.

Ponnusamy, S., Sullivan, R.D., Thiyagarajan, T., Tillmann, H., Getzenberg, R.H., and Narayanan, R. (2017a). Tissue selective androgen receptor modulators (SARMs) increase pelvic floor muscle mass in ovariectomized mice. J. Cell Biochem. *118*, 640–646.

Ponnusamy, S., Sullivan, R.D., You, D., Zafar, N., He Yang, C., Thiyagarajan, T., Johnson, D.L., Barrett, M.L., Koehler, N.J., Star, M., et al. (2017b). Androgen receptor agonists increase lean mass, improve cardiopulmonary functions, and extend survival in preclinical models of duchenne muscular dystrophy. Hum. Mol. Genet. *26*, 2526–2540.

Poulin, R., Baker, D., and Labrie, F. (1988). Androgens inhibit basal and estrogen-induced cell proliferation in the ZR-75-1 human breast cancer cell line. Breast Cancer Res. Treat. *12*, 213–225.

Robertson, J.F., Ferrero, J.M., Bourgeois, H., Kennecke, H., de Boer, R.H., Jacot, W., McGreivy, J., Suzuki, S., Zhu, M., McCaffery, I., et al. (2013). Ganitumab with either exemestane or fulvestrant for postmenopausal women with advanced, hormone-receptor-positive breast cancer: a randomised, controlled, double-blind, phase 2 trial. Lancet Oncol. *14*, 228–235.

Robinson, D.R., Wu, Y.M., Vats, P., Su, F., Lonigro, R.J., Cao, X., Kalyana-Sundaram, S., Wang, R., Ning, Y., Hodges, L., et al. (2013). Activating ESR1 mutations in hormone-resistant metastatic breast cancer. Nat. Genet. *45*, 1446–1451.

Rossi, S., Basso, M., Strippoli, A., Dadduzio, V., Cerchiaro, E., Barile, R., D'Argento, E., Cassano, A., Schinzari, G., and Barone, C. (2015). Hormone receptor status and HER2 expression in primary breast cancer compared with synchronous axillary metastases or recurrent metastatic disease. Clin. Breast Cancer *15*, 307–312.

Sasaki, T., Koivunen, J., Ogino, A., Yanagita, M., Nikiforow, S., Zheng, W., Lathan, C., Marcoux, J.P., Du, J., Okuda, K., et al. (2011). A novel ALK secondary mutation and EGFR signaling cause resistance to ALK kinase inhibitors. Cancer Res. *71*, 6051–6060.

Schneeberger, V.E., Allaj, V., Gardner, E.E., Poirier, J.T., and Rudin, C.M. (2016). Quantitation of murine stroma and selective purification of the human tumor component of patient-derived xenografts for genomic analysis. PLoS One *11*, e0160587.

Siegel, R.L., Miller, K.D., and Jemal, A. (2018). Cancer statistics, 2018. CA Cancer J. Clin. *68*, 7–30.

Sikora, M.J., Cooper, K.L., Bahreini, A., Luthra, S., Wang, G., Chandran, U.R., Davidson, N.E., Dabbs, D.J., Welm, A.L., and Oesterreich, S. (2014). Invasive lobular carcinoma cell lines are characterized by unique estrogen-mediated gene expression patterns and altered tamoxifen response. Cancer Res. *74*, 1463–1474.

Stewart, J., King, R., Hayward, J., and Rubens, R. (1982). Estrogen and progesterone receptors: correlation of response rates, site and timing of receptor analysis. Breast Cancer Res. Treat. *2*, 243–250.

Sultana, A., Idress, R., Naqvi, Z.A., Azam, I., Khan, S., Siddiqui, A.A., and Lalani, E.N. (2014). Expression of the androgen receptor, pAkt, and pPTEN in breast cancer and their potential in prognostication. Transl Oncol. https://doi.org/10.1016/j.tranon.2014.04.004.

Tentler, J.J., Tan, A.C., Weekes, C.D., Jimeno, A., Leong, S., Pitts, T.M., Arcaroli, J.J., Messersmith, W.A., and Eckhardt, S.G. (2012). Patient-derived tumour xenografts as models for oncology drug development. Nat. Rev. Clin. Oncol. *9*, 338–350.

Toropainen, S., Niskanen, E.A., Malinen, M., Sutinen, P., Kaikkonen, M.U., and Palvimo, J.J. (2016). Global analysis of transcription in castration-resistant prostate cancer cells uncovers active enhancers and direct androgen receptor targets. Sci. Rep. *6*, 33510.

Toy, W., Weir, H., Razavi, P., Lawson, M., Goeppert, A.U., Mazzola, A.M., Smith, A., Wilson, J., Morrow, C., Wong, W.L., et al. (2017). Activating ESR1 mutations differentially affect the efficacy of ER antagonists. Cancer Discov. *7*, 277–287.

Vera-Badillo, F.E., Templeton, A.J., de Gouveia, P., Diaz-Padilla, I., Bedard, P.L., Al-Mubarak, M., Seruga, B., Tannock, I.F., Ocana, A., and Amir, E. (2014). Androgen receptor expression and outcomes in early breast cancer: a systematic review and meta-analysis. J. Natl. Cancer Inst. *106*, djt319.

Vogel, V.G., Costantino, J.P., Wickerham, D.L., Cronin, W.M., Cecchini, R.S., Atkins, J.N., Bevers, T.B., Fehrenbacher, L., Pajon, E.R., Jr., Wade, J.L., 3rd, et al. (2006). Effects of tamoxifen vs raloxifene on the risk of developing invasive breast cancer and other disease outcomes: the NSABP Study of Tamoxifen and Raloxifene (STAR) P-2 trial. JAMA *295*, 2727–2741.

Wang, Q., Li, W., Liu, X.S., Carroll, J.S., Janne, O.A., Keeton, E.K., Chinnaiyan, A.M., Pienta, K.J., and Brown, M. (2007). A hierarchical network of transcription factors governs androgen receptor-dependent prostate cancer growth. Mol. Cell *27*, 380–392.

Witzel, I., Graeser, M., Karn, T., Schmidt, M., Wirtz, R., Schutze, D., Rausch, A., Janicke, F., Milde-Langosch, K., and Muller, V. (2013). Androgen receptor expression is a predictive marker in chemotherapy-treated patients with endocrine receptor-positive primary breast cancers. J. Cancer Res. Clin. Oncol. *139*, 809–816.

Yin, D., He, Y., Perera, M.A., Hong, S.S., Marhefka, C., Stourman, N., Kirkovsky, L., Miller, D.D., and Dalton, J.T. (2003). Key structural features of nonsteroidal ligands for binding and activation of the androgen receptor. Mol. Pharmacol. *63*, 211–223.

Zhao, J.C., Fong, K.W., Jin, H.J., Yang, Y.A., Kim, J., and Yu, J. (2016). FOXA1 acts upstream of GATA2 and AR in hormonal regulation of gene expression. Oncogene *35*, 4335–4344.

Zhou, Z.X., Lane, M.V., Kemppainen, J.A., French, F.S., and Wilson, E.M. (1995). Specificity of ligand-dependent androgen receptor stabilization: receptor domain interactions influence ligand dissociation and receptor stability. Mol. Endocrinol. *9*, 208–218.

ISCI, Volume *21*

Supplemental Information

Androgen Receptor Is a Non-canonical Inhibitor of Wild-Type and Mutant Estrogen Receptors in Hormone Receptor-Positive Breast Cancers

Suriyan Ponnusamy, Sarah Asemota, Lee S. Schwartzberg, Fouzia Guestini, Keely M. McNamara, Mariaelena Pierobon, Alba Font-Tello, Xintao Qiu, Yingtian Xie, Prakash K. Rao, Thirumagal Thiyagarajan, Brandy Grimes, Daniel L. Johnson, Martin D. Fleming, Frances E. Pritchard, Michael P. Berry, Roy Oswaks, Richard E. Fine, Myles Brown, Hironobu Sasano, Emanuel F. Petricoin, Henry W. Long, and Ramesh Narayanan

Transparent Methods

Reagents. TaqMan PCR primers and fluorescent probes, master mixes, Cells-to-Ct reagent, and lipofectamine were obtained from Life Technologies (Carlsbad, CA). Cell culture medium and charcoal-stripped fetal bovine serum (csFBS) were purchased from Fisher Scientific (Waltham, MA). FBS was purchased from Hyclone (San Angelo, TX). Vetspon dental cubes/sponges (Patterson Veterinary Supplies Inc., Cat. No. NC0654350) were obtained from Fisher Scientific (Waltham, MA). Details of vendors and catalog numbers are provided in the table below.

Reagent	Vendor	Catalog number
Enzalutamide	Medkoo	201821
Enzalutamide	PharmaSys	TKn20120729
AR antibody N20 Western blot	SantaCruz biotechnology	SC-816
AR antibody PG21 Western blot/IHC	Millipore	06-680
GAPDH antibody Western blot	Sigma	G8795
ER-α antibody	Cell Signaling	8644
DHT	Sigma	A8380-1G
Fulvestrant	Chemshuttle	139028
Fulvestrant	Tocris	1047
Taqman primers and probes	Life Technologies/Fisher	
pSer81 AR antibody	Millipore	07-1375
pSer118 ER antibody	Cell signaling	2511
PMA	R&D	1201/1
EGF	R&D	236-EG-200
Cell titer glo	Promega	G7572
Estradiol	Tocris	2824
Estradiol pellet	Innovative Research of America	E-121
AR antibody ChIP-Seq	Springbiosciences	E2724
FOXA1 antibody ChIP-Seq	Abcam	5089 and 23738 mixture
ER antibody ChIP-Seq	NEOMARKERS/Santa Cruz	MS-315-PABX (ER ab10 (TE111.5D11) and sc543 mixture
Lipofectamine	Life Technologies	18324012
Dual luciferase assay reagent	Promega	E1910
Ku80 antibody for IHC	Cell Signaling	2180

Cell culture. ZR-75-1 and COS7 cells were obtained from American Type Culture Collection (ATCC, Manassas, VA). Cells were cultured in accordance with the ATCC recommendations. Cell lines were authenticated by short terminal DNA repeat assay (Genetica cell line testing laboratory).

Growth assay. Cells were plated in growth medium in 96 well plates. Cells were treated for the duration indicated in the figures. Medium was changed every third day. Cell viability was measured by counting the number of cells using Coulter counter.

Tumor xenograft experiments. All animal protocols were approved by The University of Tennessee Health Science Center (UTHSC) Institutional Animal Care and Use Research Committee (IACUC). Xenograft experiments were performed as previously published (Narayanan et al., 2014)**.** Wherever ovariectomy was described, the animals were ovariectomized in the institution under anesthesia and in accordance with the IACUC approved protocol. HCI-7, HCI-9, and HCI-13 (invasive lobular breast cancer) PDXs were kindly provided by Dr. Alana Welm (Huntsman Cancer Institute, Salt Lake City, Utah). HCI PDX tumor fragments (1 mm^3) were surgically implanted under the mammary fat pad in female NOD SCID Gamma (NSG) mice. HCI-7 PDX was performed in animals that were ovariectomized and supplemented with estradiol pellet. HCI-9 and HCI-13 PDX was performed in intact animals that were not ovariectomized. Tumor volume was measured once or twice weekly for HCI PDXs depending on their growth properties. At the end of the study, animals were sacrificed and tumors were excised, weighed, and stored for various analyses. HCI-7 PDX were performed twice, while HCI-13 PDX was performed five times. All the experiments reproduced the representative results shown in this manuscript.

Patient specimen collection. Specimens from breast cancer patients were collected with patient consent under a protocol approved by the UTHSC Institutional Review Board (IRB). The protocol number for the IRB approval is 14-03113XP. Specimens were collected immediately after surgery in RPMI medium containing penicillin:streptomycin and Fungizone and transported to the laboratory on ice. The tissues were finely minced and treated with collagenase for 2 hours. The digested tissues were washed with serum-free medium and frozen in liquid nitrogen in freezing medium (5% DMSO+95% FBS) or implanted under the mammary fat pad in female NSG mice.

Sponge culture. Patient specimens frozen in liquid nitrogen in freezing medium were used for sponge culture. Sponge cultures were performed in accordance with the protocol published earlier (Dean et al., 2012; Hu et al., 2016; Ochnik et al., 2014)**.** Tumors were sliced into small pieces (~1 mm^3) and incubated on pre-soaked gelatin sponges (5 fragments/sponge) in 12 well plates containing 1.5 mL medium (MEM+10% FBS+2 mM L-glutamine+10 µg/mL insulin+10 µg/mL hydrocortisone + penicillin: streptomycin). The cultures were performed in triplicates. Pooled samples (n=5 fragments/sponge) from each sponge constituted one sample. Medium was replaced the next day and treated as indicated in the figures. Tissues were harvested after 3 days of treatment, RNA extracted, and expression of various genes measured. Characteristics of the patient specimens used in PDX and in sponge cultures are provided in **Table ST1**.

Microarray. RNA from tumors was extracted and verified qualitatively and quantitatively. Total RNA (200 ng/sample; n=4/group) from each sample was amplified and labeled using the WT Plus

Kit from Affymetrix and processed according to Affymetrix protocol. The arrays (Human ST2.0, Affymetrix, Santa Clara, CA) were washed and stained on Affymetrix Fluidics station 450 and scanned on an Affymetrix GCS 3000 scanner.

Data from microarrays were normalized using Affymetrix Expression Console. Mean, Standard Deviation, and Variance were calculated across the groups. Fold Change from vehicle-treated samples was calculated, and a fold change of 1.5 was used as cutoff. Student's t-test was used to determine the significance and a cutoff of p value < 0.05 was used for significance discovery. False discovery rate was calculated using Benjamini & Hochberg method, and a cutoff for FDR < 0.05 was used to create a significant differential expression list. The gene candidate list was loaded to Ingenuity Pathway Analysis. Microarray experiments were performed at the UTHSC Molecular Resources Center (MRC), and data analysis was performed by the UTHSC Molecular Bioinformatics core facility.

Chromatin immunoprecipitation assay (ChIP) -Sequencing (ChIP-Seq). HCI-13 xenograft specimens were snap frozen and stored for ChIP-sequencing analysis. ChIP-Seq study was performed in vehicle or enobosarm-treated HCI-13 PDX grown in NSG mice. ChIP was performed with ER, AR, or FOXA1 (n=3-5/group) antibodies and genome-wide sequencing were performed on a NextSeq 500 sequencer. For ChIP, the protocol was based on existing procedures (Carroll et al., 2005) with some modifications. Briefly, the frozen xenograft tumors were sectioned and bifunctional cross-linking was performed at room temperature with 2 mM dissuccinyl glutarate (DSG) for 45 minutes followed by 10 minutes fixation with 1 % methanol-free formaldehyde. A standard SDS-based protocol was used, whole lysates were made from the tissues and were

sonicated using a Covaris E220 machine (Covaris Inc., Woburn, MA), for 20 minutes per sample (settings: 10% duty factor, 175 peak intensity power at 200 cycles per burst). ER, AR, or FOXA1 was immunoprecipitated, washed, and the complex eluted. The DNA-protein complex was reverse cross-linked by treating with proteinase K (1 µg/µl) and incubating at 65°C for 6 hours to overnight. After reverse cross-linking, precipitated and input DNA was purified using Minielute PCR purification columns (Qiagen).

For library preparation, Accel-NGS 2S Plus Library Kit (Swift Biosciences, Ann Arbor, MI) was used. For each library 2-10 ng DNA was used. After amplification, fragments of 200-600 bp were selected and cleaned using AmPure XP beads (Beckman Coulter, Indianapolis, IN) and analyzed on a Fragment Analyzer (Advanced Analytical, Ames, IA). For sequencing, NextSeq 500 sequencing platform (Illumina, San Diego, CA) was used. Human genome build 19 (hg19) was used as the reference genome. Sequencing data from ChIP experiments were aligned to the human genome using Bowtie (Langmead et al., 2009). For peak calling MACS2 was used (Feng et al., 2012). Significance is defined as regions that are greater than or less than 2 fold different in enobosarm-treated samples compared to vehicle-treated samples and had a $q<0.05$ for ER, and $q<0.05$ for AR and FOXA1.

Data and software availability: Accession number for the sequencing data from public deposition is GSE128018. Microarray data was deposited in GEO and the accession number is GSE126318.

Statistics: Statistical analysis was performed using GraphPad prism software (La Jolla, CA). Experiments containing two groups were analyzed by simple t-test, while those containing more than two groups were analyzed by one-way analysis of variance (ANOVA) followed by Tukey

post-hoc test. Microarray, phospho-proteomics, and ChIP-Seq statistical analyses are described under the respective methods.

All *in vitro* experiments were performed at least in triplicate with each treatment having an n=3. Data are represented as mean ± S.E. Statistics are represented as * $p<0.05$, ** $p<0.01$, *** $p<0.001$.

Serum drug concentration measurement. Blood was collected 24-30 hours after the last dose and serum was separated. One hundred microliters of serum was mixed with 200 µl of Acetonitrile/Internal Standard and added to the plates. A serial dilutions of the respective drug standards were prepared in 100 µl of rat serum with concentrations ranging 1000, 500, 250, 125, 62.5, 31.2, 15.6, 7.8, 3.9, 1.9, .97 and 0 nM. Standards were extracted with 200 µl of Acetonitrile/Internal Standard and added to 96 well plates. The analysis of the drugs was performed using LC-MS/MS system consisting of Shimadzu Nexera X2 HPLC with an AB/Sciex Triple Quad 4500 Q-Trap™ mass spectrometer. The separation was achieved using a C_{18} analytical column (Alltima™, 2.1 X 100 mm, 3 µm) protected by a C_{18} guard column (Phenomenex™ 4.6mm ID cartridge with holder). Various parameters are provided in the table below.

	Enobosarm	**DHT**	**Enzalutamide**	**Fulvestrant**
Run time (min)	2.5	4.0	6.0	2.5
Injection volume (µl)	10	10	10	10
Mobile phase				
Channel A	95% acetonitrile + 5% water + 0.1% formic acid	100% methanol + 0.1% formic acid	95% acetonitrile + 5% water + 0.1% formic acid	100% acetonitrile + 0.1% formic acid
Channel C	95% water + 5% acetonitrile + 0.1 % formic acid	100% water + 0.2% formic acid	95% water + 0.1% formic acid + 5% water	100% water
A:B (%)	5:95	70:30	30:70	20:80
Mode	Negative	Positive	Positive	Negative

Declustering Potential (DP)	-190	31	101	-150
Collision Energy (CE)	-34	25	41	-38
Cell Exit Potential (CXP)	-9	10	12	-19
m/z	362.29/184.6	291/255.2	465/209.1	605.2/427

Transfection. Transient transactivation studies were conducted in COS7 cells. Briefly, COS7 cells were plated in DME+5%csFBS w/o phenol red medium in 24 well plates. Cells were transfected with 0.25 μg ERE-E1b-LUC or pS2-LUC, pCR3.1 human ER-α (all three plasmids were gifts from Dr. Carolyn Smith, Baylor College of Medicine, Houston, TX), and CMV-renilla-LUC using lipofectamine reagent (Life Technologies). Cells were treated 24 hours after transfection and luciferase assay was performed 48 hours after transfection. Firefly luciferase values were normalized to renilla luciferase numbers.

ER-LBD competitive binding assay. ER-LBD competitive binding assay was performed as previously described [1].

Immunohistochemistry: Fourteen cases of invasive breast cancer, luminal B subtype, were chosen randomly from the formalin fixed paraffin embedded samples available from the tissue bank of the pathology department of Tohoku University Hospital. The luminal B classification of these samples was on the basis of having ERα expression greater than 1% and a Ki-67 labelling index of greater than 20 percent. The samples had variable levels of PR expression (Labelling Index, Average 48.9, Range 0-100) and other clinicopathological characteristics (Ki67, Average 38%, Range 20-48%; Nottingham Grade, I n=1, II n=10, III n=3). The use of these samples was

approved by the Tohoku University School of Graduate Medicine Ethic review board (2014-1-107). Blocks of tissue were retrieved and sectioned at a thickness of 3 μM and mounted on glass slides. In order to asses co-localization mirror image sectioning was used. The slides were then stained for ERα and AR (ERα, 1:50 dilution, Clone 6F11, Leica ; AR , 1:50 dilution, Clone AR441, Dako) using immunohistochemistry as previously described [2,3]. In order to determine the proportion of stroma and epithelia in xenografts, H&E staining of FFPE sections was undertaken. The slides were then analyzed both by a trained and experienced pathological researcher and digitally using Image J who was blind as to the ID of the sections. In brief, initially the slides were read by an experienced pathology researcher, the percentage stroma estimated and a representative photomicrograph taken. The color threshold function of Image J was used manually to define stromal areas on this photomicrograph and area as a percentage of total cellular area was calculated using the histogram function.

Gene expression. RNA extraction and cDNA preparations were performed using cells-to-ct kit. Gene expression studies were performed using TaqMan probes on ABI 7900 realtime PCR machine. For gene expression studies in cells, cells were plated in 96 well plates in charcoal-stripped serum containing medium. Cells were maintained in this medium for two days and then treated as indicated in the figures. RNA was extracted and cDNA synthesized using cells-to-ct-kit. Gene expression studies in tumor xenografts were performed by extracting the RNA using RNA-isolation kit from Qiagen. cDNA was synthesized and the expression of genes was quantified by realtime PCR using TaqMan primers and probes.

Western blotting. Tumors were added to appropriate volume of lysis buffer containing protease and phosphatase inhibitors and were completely disintegrated using bead-based fragmentation method using FastPrep FP120 (Thermo). Protein was extracted by three freeze-thaw cycles. Equal amounts of protein were fragmented on a SDS-PAGE and transferred to a nitrocellulose membrane. Western blot for various proteins was performed by standard method.

Detailed immunohistochemistry protocol for ki67, AR, and ER.

Day 1:

Note: The slides were placed in a rack and the following steps were performed. The paraffin was melted with heat until total melted using hair dryer.

A) Deparaffinize and rehydrate:

1. Xylene: 2 x 10 minutes
2. Xylene: 2 x 5 minutes
3. 100% ethanol: 1 minutes
4. 95% ethanol: 1 minutes
5. 70 % ethanol: 1minutes
6. 50 % ethanol: 1 minutes
7. Running cold tap water to rinse.

B) Antigen retrieval

Prepare: 1 ml of citrate Buffer (Citrate buffer 1M pH 6.0) + 100 ml distilled water

8. The slides were placed in a rack with citrate solution and autoclaved for 5 minutes at 121°C.
9. The rack was taken out and cooled down for 20 minutes in crushed ice.
10. Washed three times with PBS.

C) Blocking buffer & Primary antibody

11. The slides were drained and 2-3 drops of blocking buffer was applied (Goat, Histofine SAB-PO kit; Nichirei, Tokyo, Japan) and incubated at room temperature for 30 minutes in a humid chamber.

12. The slides were drained and 55 µl of primary antibody (mouse, monoclonal antibody, diluted 1/50 in BSA 0.5- NaN_3 0.05%-PBS for AR and ERα, and diluted at 1/100 for KI67, Rabbit polyclonal antibody) was added and incubated overnight at 4°C in humid chamber.

Note: **AR** monoclonal mouse antibody, clone AR441, DAKO.
ERα monoclonal mouse antibody, clone 6F11, Leica [NCL-L-ER-6F11].
KI67 monoclonal mouse antibody, clone MIB-1, DAKO M7240

Day 2:

D) Block endogenous peroxidases

13. The following day, the slides were washed three times in PBS.
14. Slides were soaked in a new rack filled with 0.3% H_2O_2 solution (50 ml methanol + 0.5 ml H_2O_2) for 30 minutes at room temperature.

E) Secondary antibody

15. Washed three times with PBS.
16. The slides were dried and 2-3 drops of secondary antibody (same specie as primary antibody) was added, and incubated in humid chamber for 30 minutes at room temperature.

F) Revelation with DAB

17. Rinsed with PBS three times.
18. The slides were dried and 2-3 drops of Streptavidin-Peroxidase was added and incubated 30 minutes at room temperature.
19. The slides were washed with PBS three times and plunged them 3-5 minutes in DAB solution for the revelation (10ml Tris-buffer 0.25M pH 7.0+ DAB 13mg solution complete to 50ml distilled water + 20 µl H_2O_2).

G) Counterstaining

20. Rinsed with tap water and counterstained in hematoxylin 4 minutes.
21. Rinsed with running tap water.

H) Dehydration

22. Rinsed with running tap water
23. Immediately dehydrated slides in 95% ethanol (2x), 100% ethanol (2x), cleared in 4 baths of xylene.

I) Mounting the slides:

24. The slides were mounted using an automatic cover slipper (Tissue Tek Glas, Sakura)

Hematoxylin Eosin staining

1. The wax was melted using hair dryer.
2. The wax was removed in successive baths of xylene 2 x 10 minutes, 2 x 5 minutes.
3. Hydrated in 4 baths of ethanol 1 minute each (100%, 95%, 70%, 50%).
4. Rinsed with tap water in a bucket.
5. The slides were immersed in Hematoxylin Carazzi for 30 minutes.
6. Washed with running tap water.
7. Immersed quickly 3 times in 1% HCl-alcohol bath.
8. Rinsed in distilled water for 5 minutes.
9. Stained with 1% eosin for 15 seconds.
10. Washed in tap water then proceeded to four baths in ethanol, then four in xylene.
11. The slides were mounted using automatic cover slipper machine (Tissue Tek Glass, SAKURA).

IHC-PARAFFIN PROTOCOL

Ku80

Day 1:

Note 1 : The slides were placed in a rack and the paraffin was melted with heat until total melted using hair dryer.

Note 2: Positive control: Human colon cancer.

B) Deparaffinize and rehydrate:

8. Xylene: 2 x 10 minutes
9. Xylene: 2 x 5 minutes
10. 100% ethanol: 1 minutes
11. 95% ethanol: 1 minutes
12. 70 % ethanol: 1minutes
13. 50 % ethanol: 1 minutes

14. Running cold tap water to rinse.

B) Antigen retrieval

Prepare: 1 ml of citrate Buffer (Citrate buffer 1M pH 6.0) + 100 ml distilled water

8. The slides were placed in a rack with citrate solution and autoclave for 5 minutes at 121°C.
9. The rack was taken out and cooled down for 20 minutes in crushed ice.
10. Washed three times with PBS.

C) Blocking buffer & Primary antibody

11. The slides were drained and 2-3 drops of blocking buffer (Goat, Histofine SAB-PO kit; Nichirei, Tokyo, Japan) was applied, incubated at room temperature for 30 minutes in a humid chamber.
12. The slides were drained and 55 µl of primary antibody (Rabbit, monoclonal antibody, diluted 1/150 in BSA 0.5- NaN_3 0.05%-PBS) was added. Incubated overnight at 4°C in humid chambers

Note: **Ku80** monoclonal Rabbit antibody, clone C48E7, Cell signaling Technology #2180

Day 2:

D) Block endogenous peroxidases

13. The following day, the slides were washed three times in PBS.
14. The slides were soaked in a new rack filled with 0.3% H_2O_2 solution (50 ml methanol + 0.5 ml H_2O_2) for 30 minutes at room temperature.

E) Secondary antibody

15. Washed three times with PBS.
16. The slides were dried and 2-3 drops of secondary antibody (same specie as primary antibody Rabbit) were added, and incubated in humid chamber for 30 minutes at room temperature.

F) Revelation with DAB

17. Rinsed with PBS three times.
18. The slides were dried and 2-3 drops of Streptavidin-Peroxidase was added and incubated 30 minutes at room temperature.

19. The slides were washed with PBS three times and plunged them 4 minutes in DAB solution for the revelation (10ml Tris-buffer 0.25M pH 7.0+ DAB 13mg solution complete to 50ml distilled water + 20 µl H_2O_2).

G) Counterstaining

20. Rinsed with tap water and counterstain in hematoxylin 3 minutes.
21. Rinsed with running tap water.

H) Dehydration

22. Rinsed with running tap water
23. Immediately the slides were dehydrated in 95% ethanol (2x), 100% ethanol (2x), and clear in 4 baths of xylene.

I) Mounting the slides:

24. The slides were mounted using an automatic cover slipper (Tissue Tek Glas, Sakura)

Reagents:

A) Phosphate Buffer Saline PBS 0.01M

NaH_2PO_4. $2H_2O$	4.5g
Na_2HPO_4. 12H2O	32.27g
NaCl	80g

B) Bovine Serum Albumin BSA

BSA	1g
10% NaN_3	1ml
0.01M PBS	200ml

C) 1 M Citrate Buffer pH 6.0

A: Citric Acid monohydrate	21g – distilled water 100ml
B: Trisodium citrate dehydrate	147g – distilled water 500ml
Mix A 90ml + B 410 ml	

C) DAB

0.05 M Tris buffer (0.25M tris buffer 40 ml + 160 ml distilled water)	200ml
DAB	1 g

Notes:

- The monoclonal antibody Ku80 detects the endogenous levels of total protein, nuclei localized.

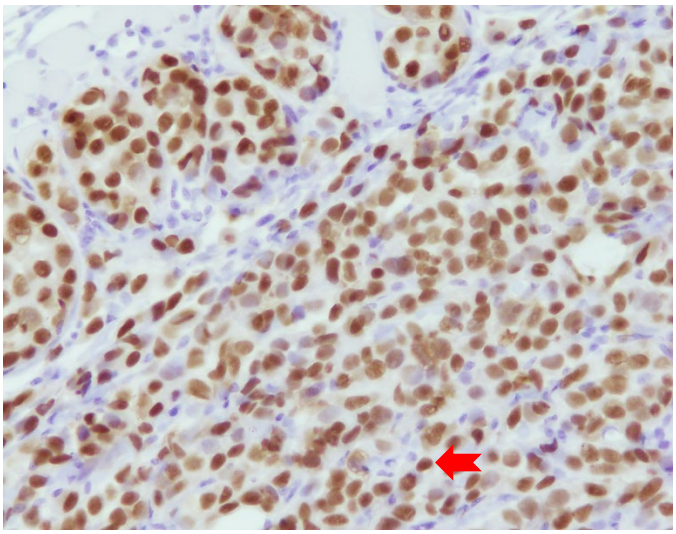

- In the human colon cancer positive control, the antibody stains positively the nuclei of epithelial cells, carcinoma and stroma cells (fibroblast, lymphocytes)

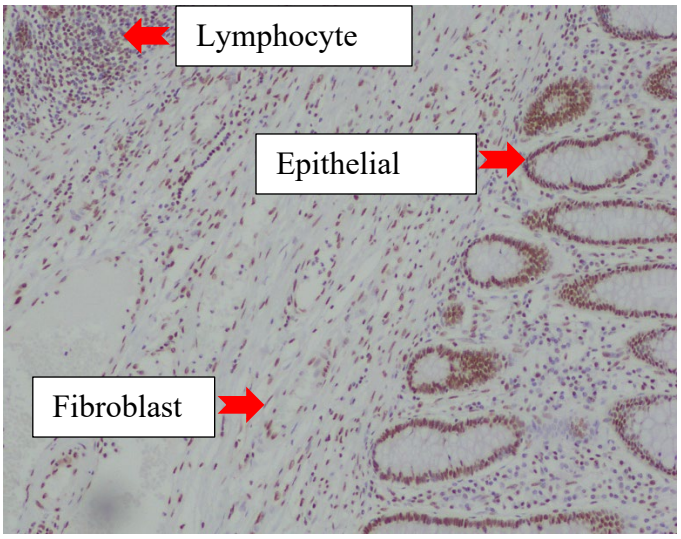

- In the PDx vehicle samples, the antibody stains positively the nuclei of human carcinoma cells, and not the stroma.

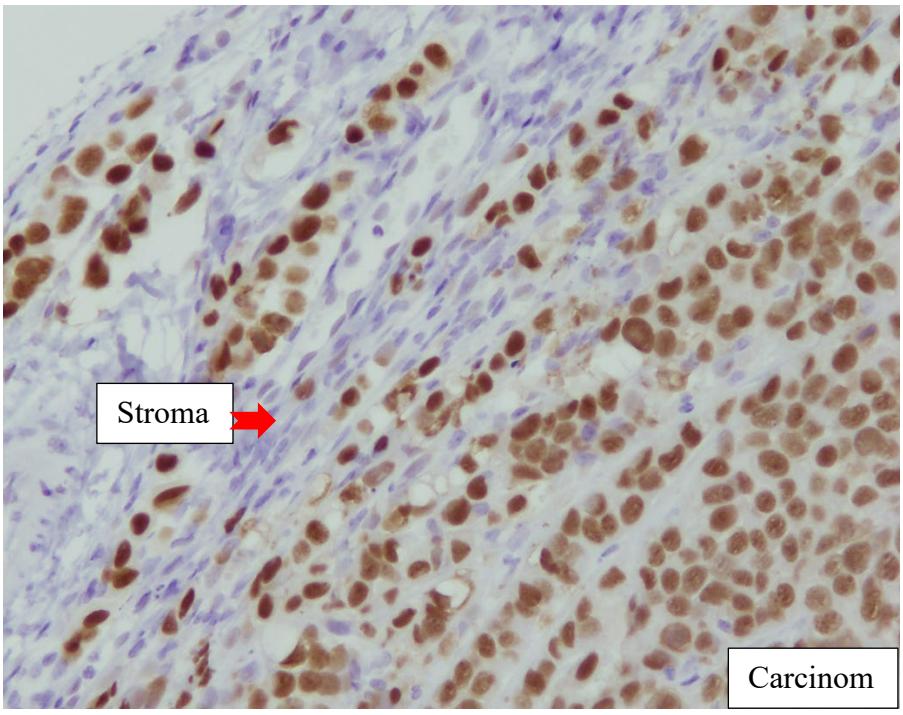

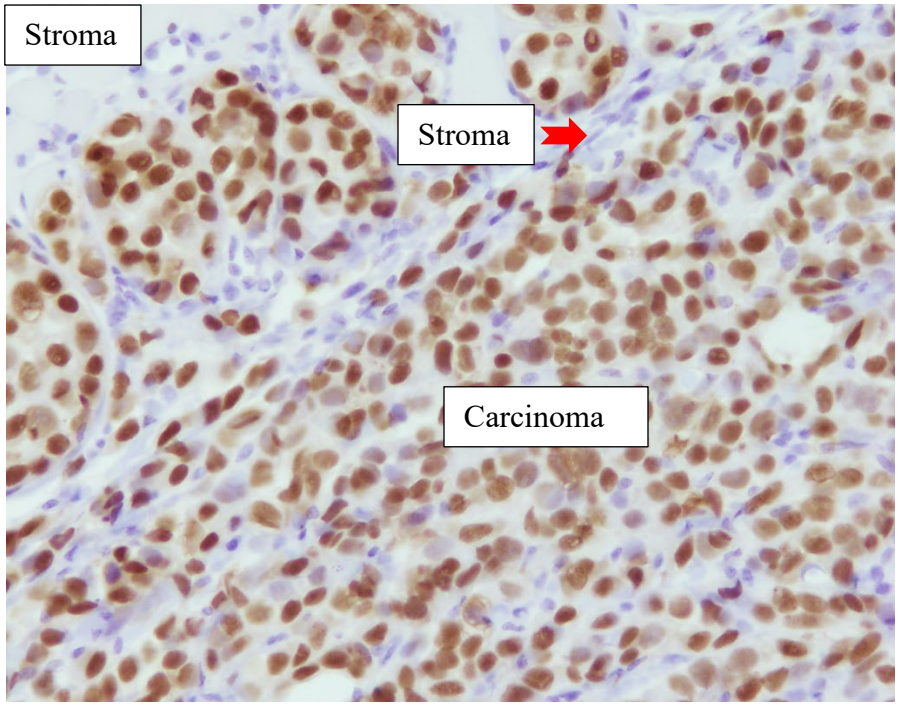

Reverse-phase protein array (RPPA)-based protein pathway activation mapping. Frozen samples from HCI-13 PDX treated with vehicle or enobosarm were cut into 8 µm cryosections and mounted on uncharged glass slides. Whole tissue lysates were directly prepared from the tissue sections using a 1:1 mixture of T-PER (Tissue Protein Extraction Reagent; Pierce, Rockford, IL) and 2X Tris-Glycine SDS Sample Buffer (Invitrogen, Carlsbad, CA) supplemented with 5% 2-mercaptoethanol [4]. Samples were boiled for 8 minutes and stored at -80°C until arrayed.

Samples and standard curves for internal quality assurance were printed onto nitrocellulose-coated slides (Grace Bio-labs, Bend, OR) using an Aushon 2470 arrayer (Aushon BioSystems, Billerica, MA). Selected arrays were used to estimate the amount of protein in each sample using a Sypro Ruby Protein Blot Stain (Molecular Probes, Eugene, OR) protocol following manufacturer's instructions [4]. Remaining arrays were tested with a single primary antibody using an automated system (Dako Cytomation, Carpinteria, CA) as previously described [5]. Arrays were first incubated with Reblot Antibody stripping solution (Chemicon, Temecula, CA), followed by two washes in PBS, and I-block solution (Tropix, Bedford, MA) for 4 hours. Arrays were probed with a total of 174 antibodies targeting a wide range of protein kinases and their activation via phosphorylation (**Table ST2**). Antibodies specificity was tested using standard immunoblotting on a panel of cell lysates [4,6]**.** Selected arrays were stained with an anti-rabbit or anti-mouse biotinylated secondary antibody alone (Vector Laboratories Inc., Burlingame, CA and Dako Cytomation, Carpinteria, CA, respectively) and used as negative controls for non-specific binding/background subtraction.

The commercially available Signal Amplification System (CSA; Dako Cytomation) and a streptavidin-conjugated IRDye 680 secondary antibody (LI-COR Biosciences, Lincoln, NE) were used as signal detection methods. Images were acquired on the laser-based PowerScanner (TECAN, Mönnedorf, Switzerland), and data were analyzed using the MicroVigene software

Version 5.1 (Vigene Tech, Carlisle, MA) as previously described [5]. Intra and inter-assay reproducibility have been previously reported [7,8].

References:

1 Yepuru, M. *et al.* Estrogen receptor-{beta}-selective ligands alleviate high-fat diet- and ovariectomy-induced obesity in mice. *J Biol Chem* **285**, 31292-31303, doi:10.1074/jbc.M110.147850 (2010).

2 McNamara, K. M. *et al.* Androgenic pathway in triple negative invasive ductal tumors: its correlation with tumor cell proliferation. *Cancer Sci* **104**, 639-646, doi:10.1111/cas.12121 (2013).

3 Niikawa, H. *et al.* Intratumoral estrogens and estrogen receptors in human non-small cell lung carcinoma. *Clin Cancer Res* **14**, 4417-4426, doi:10.1158/1078-0432.CCR-07-1950 (2008).

4 Pin, E., Federici, G. & Petricoin, E. F., 3rd. Preparation and use of reverse protein microarrays. *Curr Protoc Protein Sci* **75**, Unit 27 27, doi:10.1002/0471140864.ps2707s75 (2014).

5 Baldelli, E. *et al.* Functional signaling pathway analysis of lung adenocarcinomas identifies novel therapeutic targets for KRAS mutant tumors. *Oncotarget* **6**, 32368-32379, doi:10.18632/oncotarget.5941 (2015).

6 Signore, M. & Reeder, K. A. Antibody validation by Western blotting. *Methods Mol Biol* **823**, 139-155, doi:10.1007/978-1-60327-216-2_10 (2012).

7 Rapkiewicz, A. *et al.* The needle in the haystack: application of breast fine-needle aspirate samples to quantitative protein microarray technology. *Cancer* **111**, 173-184, doi:10.1002/cncr.22686 (2007).

8 Pierobon, M. *et al.* Pilot phase I/II personalized therapy trial for metastatic colorectal cancer: evaluating the feasibility of protein pathway activation mapping for stratifying patients to therapy with imatinib and panitumumab. *J Proteome Res* **13**, 2846-2855, doi:10.1021/pr401267m (2014).

Figure S1

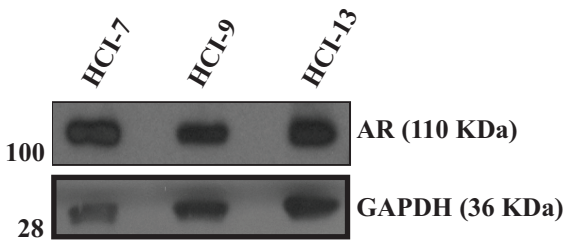

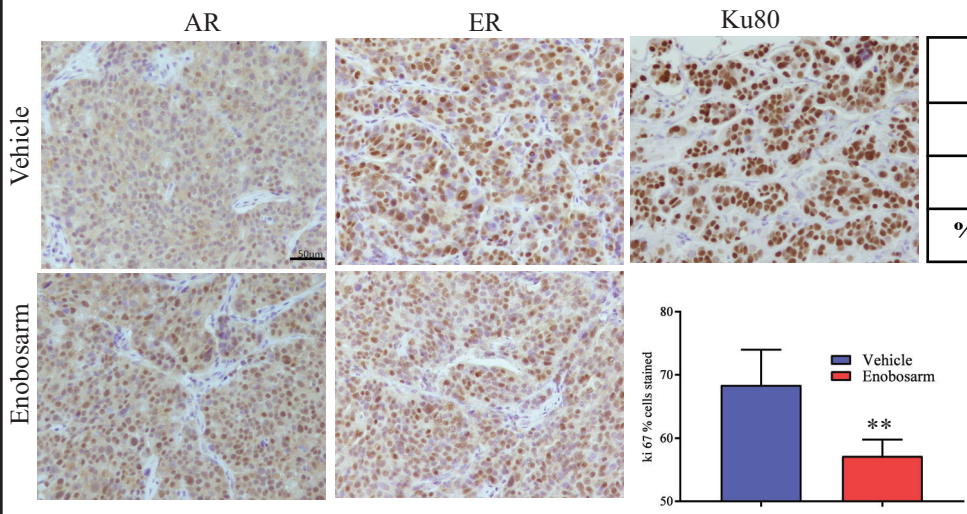

	HCI-7 (n=5/group) Vehicle	
	Avg.	S.E.
% stroma	8.5	1.83
% epithelium	91.5	1.83

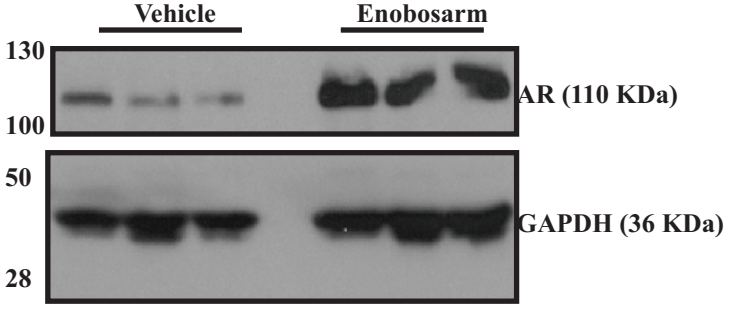

Figure S1: HCI-7 PDX characteristics (related to Figure 1). AR expression shown by Western blot in HCI-7, HCI-9, and HCI-13 PDXs. HCI-7 tumors from animals treated with vehicle or enobosarm (**Figure 1C**) were formalin-fixed and immunostained with the indicated antibodies. Representative images of n=4-5/group/stain are shown. Scale is provided in a representative image (50 μm). Ki-67 staining was quantified and represented as bar graph (n=5/group). AR and GAPDH Western blots in HCI-7 tumors from animals treated with vehicle or enobosarm is provided on the right. * $p<0.05$. AR-androgen receptor; ER-estrogen receptor; SARM-selective androgen receptor modulator; SRB-sulforhodamine B; mpk-milligram per kilogram body weight. Values are expressed as average ± S.E. from n=3-4/data point.

Figure S2

A

Drug	Concentration (nM) (n=4/group)	
	Avg.	S.E.
Enobosarm	102102	3554
Enzalutamide	15398	1374
DHT	180	57
Fulvestrant	6399	1209

B

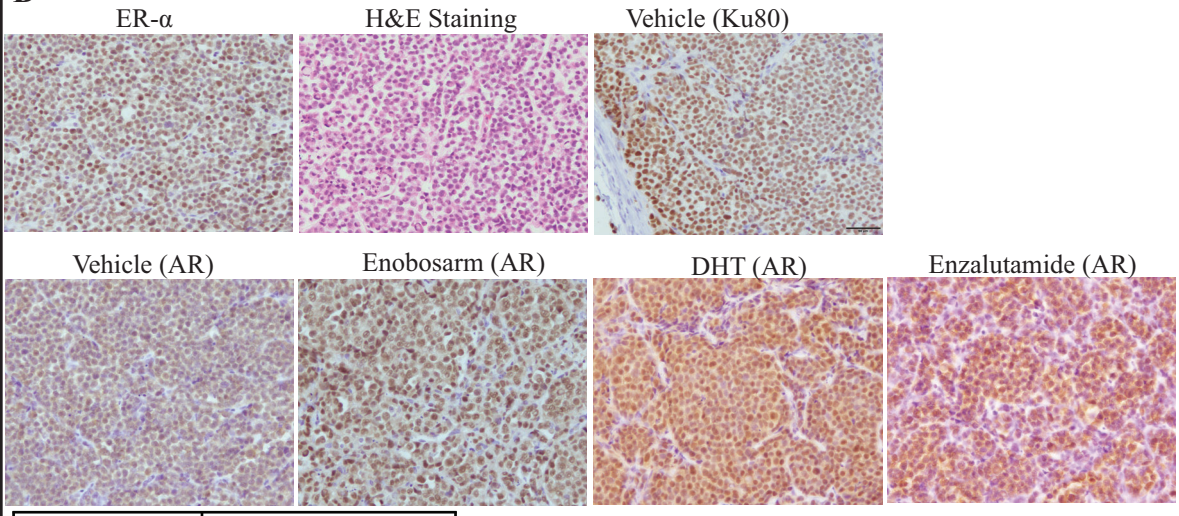

	HCI-13 (n=6/group) Vehicle	
	Avg.	S.E.
% stroma	16.3	2.97
% epithelium	83.7	2.97

C

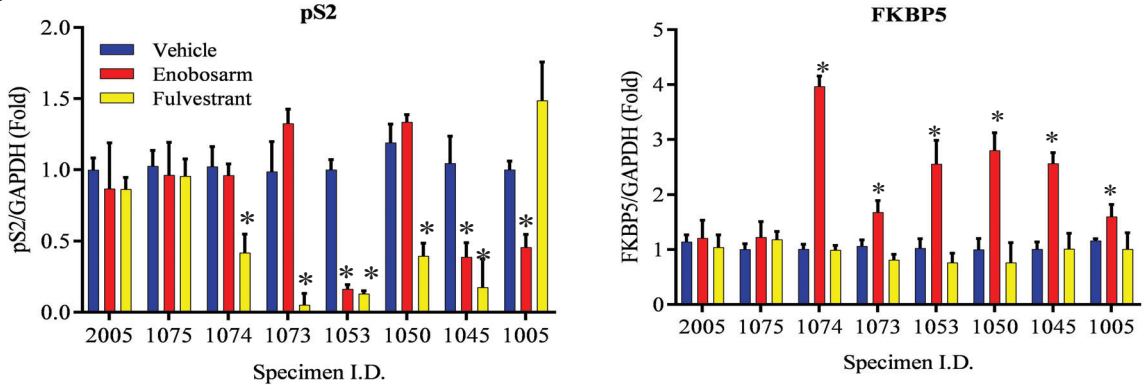

Figure S2: **HCI-13 PDX characteristics (related to Figure 1). A**. Drug concentration in the serum of HCI-13 tumor-bearing animals that were treated with enobosarm, enzalutamide, DHT, or fulvestrant using LC-MS/MS (n=4/group). **B**. HCI-13 tumors from animals treated with various drugs were formalin-fixed and immunostained with the indicated antibodies. Representative images of n=5/group/stain are shown. Scale is provided in a representative image (50 μm). Percent stromal and epithelial cells are shown in the table below. **C**. *Effect of enobosarm on ER-positive breast cancer patient specimens*. Breast cancer specimens obtained from patients were cultured on gelatin sponges (n=3; each n was obtained from 5 tumor fragments) in full serum containing growth medium. Tissues were treated with vehicle, 1 μM enobosarm, or 100 nM fulvestrant for three days. RNA was extracted from the tissues and expression of genes was measured by real time PCR and normalized to GAPDH.

Figure S3

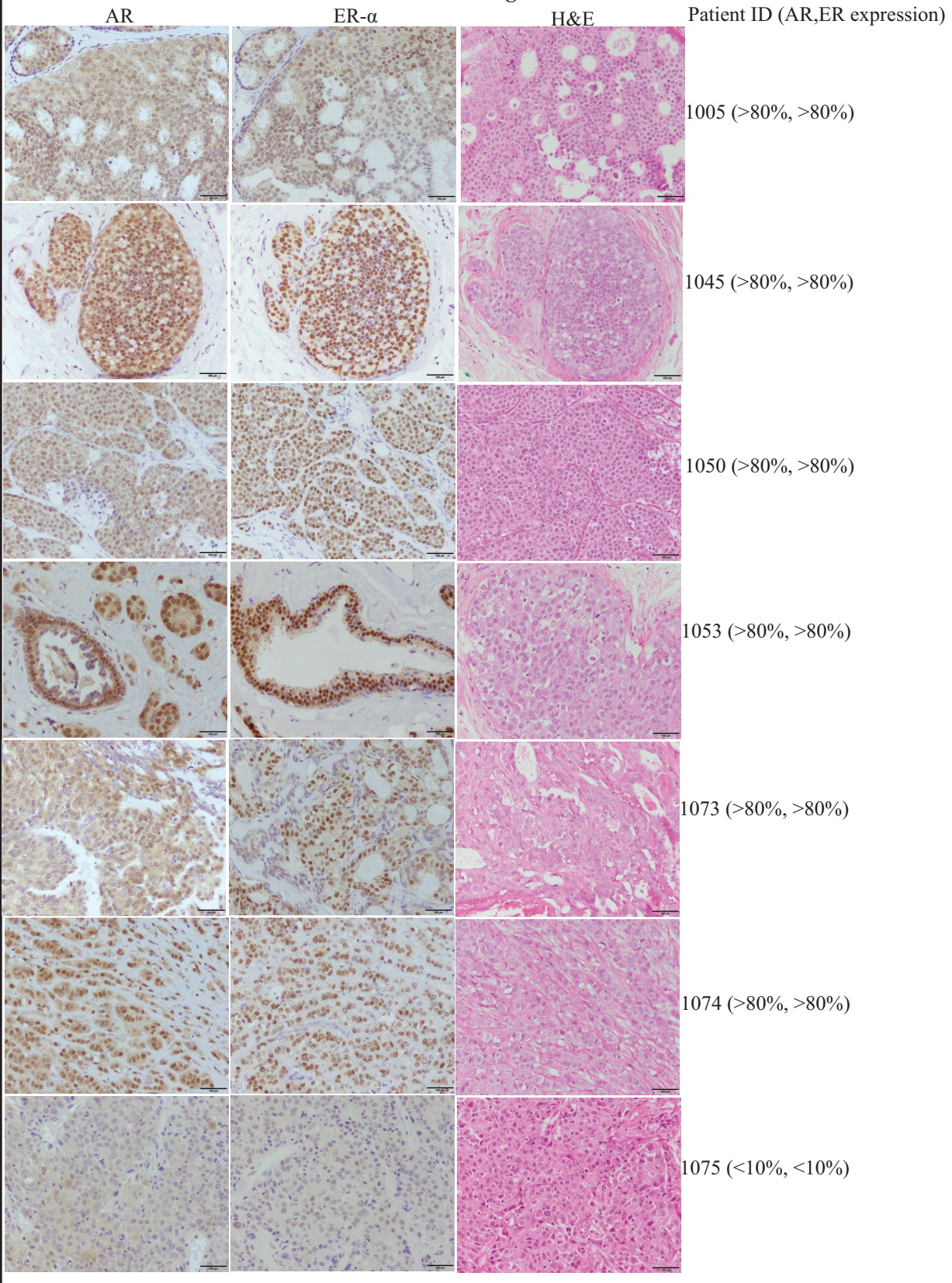

Figure S3 (Related to Figure 1). Immunohistochemistry staining of patient specimens for AR, ER, and H&E staining. The numbers to the right of each stain indicates the patient ID and the percent cells stained for AR and ER. Scale is provided in a representative image (100 μm).

Figure S4

A

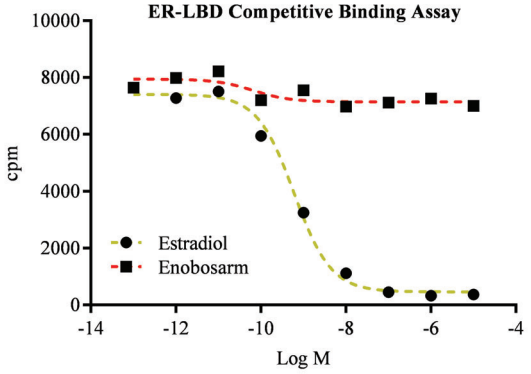

B

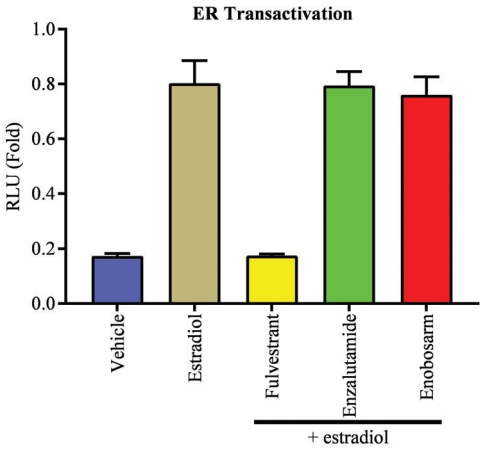

Figure S4 (Related to Figure 3). **A**. ER-LBD competitive binding assay. ER-LBD protein made from bacterial expression plasmid was incubated overnight at 4°C with 1 nM ^{3}H estradiol and increasing concentrations of cold estradiol or enobosarm. Amount of radioactive estradiol incorporated in the ER LBD (measure of the amount displaced by a cold ligand) is determined using scintillation counter. **B**. AR ligands have no effect on ER transactivation. 25 ng pCR3.1 hER-α, 0.25 µg pS2-LUC, and 10 ng CMV renilla-LUC were transfected into COS7 cells using lipofectamine. Cells were treated 24 hours after transfection with 0.1 nM estradiol alone or in combination with 100 nM fulvestrant, 10 µM enobosarm, or 10 µM enzalutamide. Luciferase assay was performed 48 hours after transfection. Firefly luciferase values were normalized to renilla luciferase values (n=3/treatment).

Figure S5

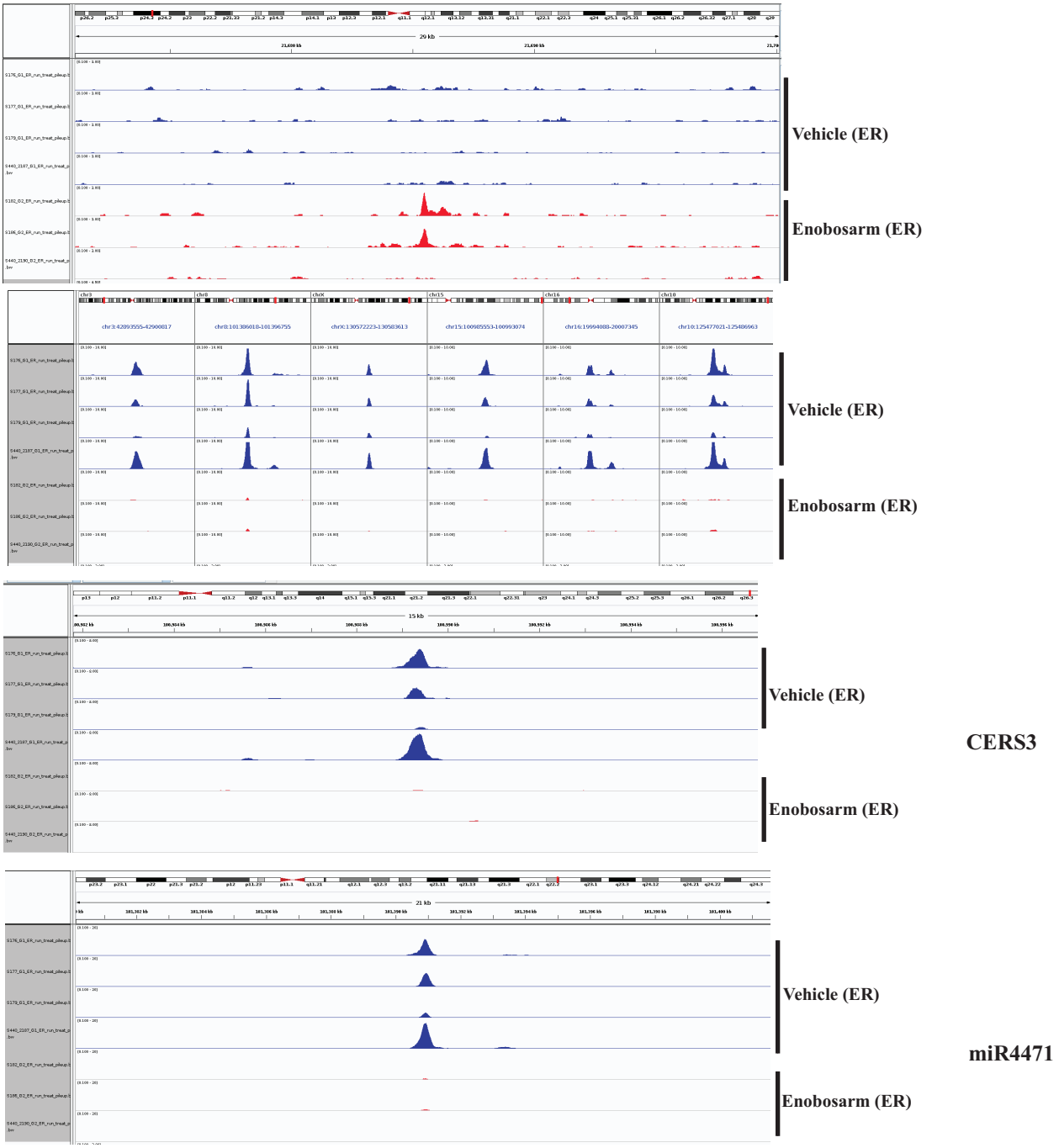

Figure S5 (Related to Figure 3): Representative ER ChIP-Seq peaks in the regulated regions of genes. Venn diagram of overlapping sites.

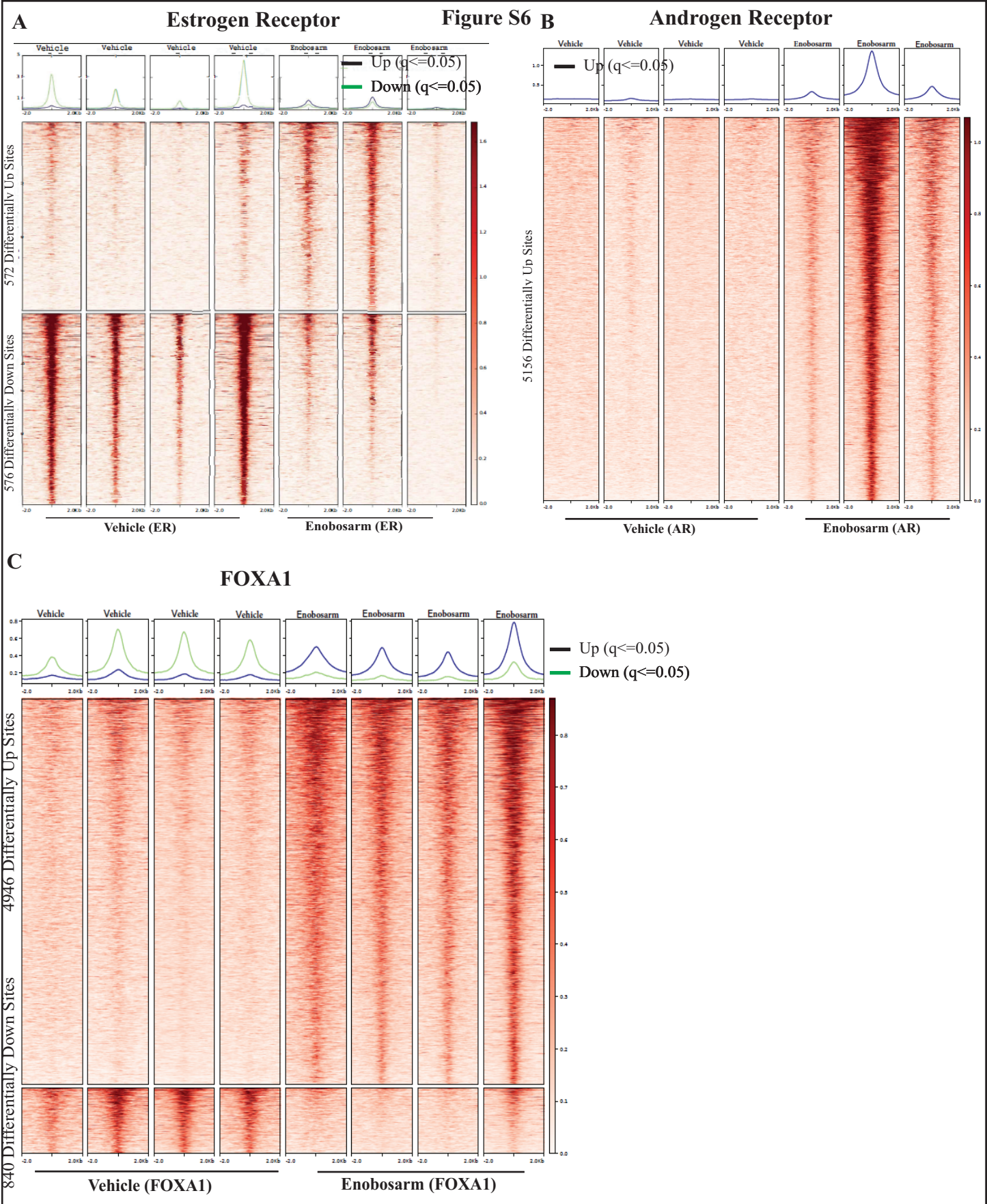

Figure S6 (Related to Figures 3,4, and 5): Heatmap of ER (A), AR (B), and FOXA1 (C) ChIP-Seq of individual tumor specimens that are represented as averages in figures 3, 4, and 5, respectively.

Figure S7

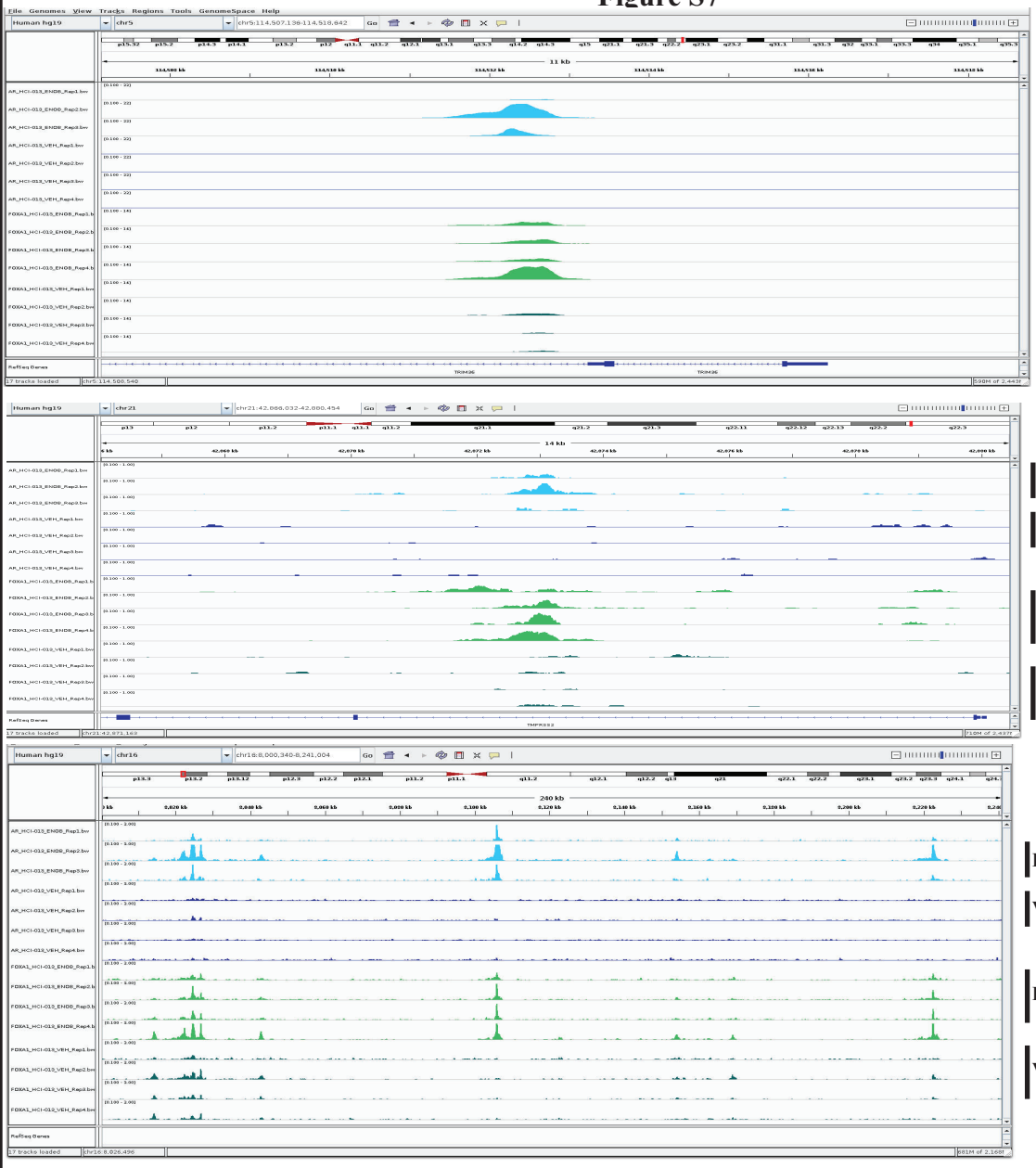

Figure S7 (Related to Figures 4 and 5): Representative AR and FOXA1 ChIP-Seq peaks.

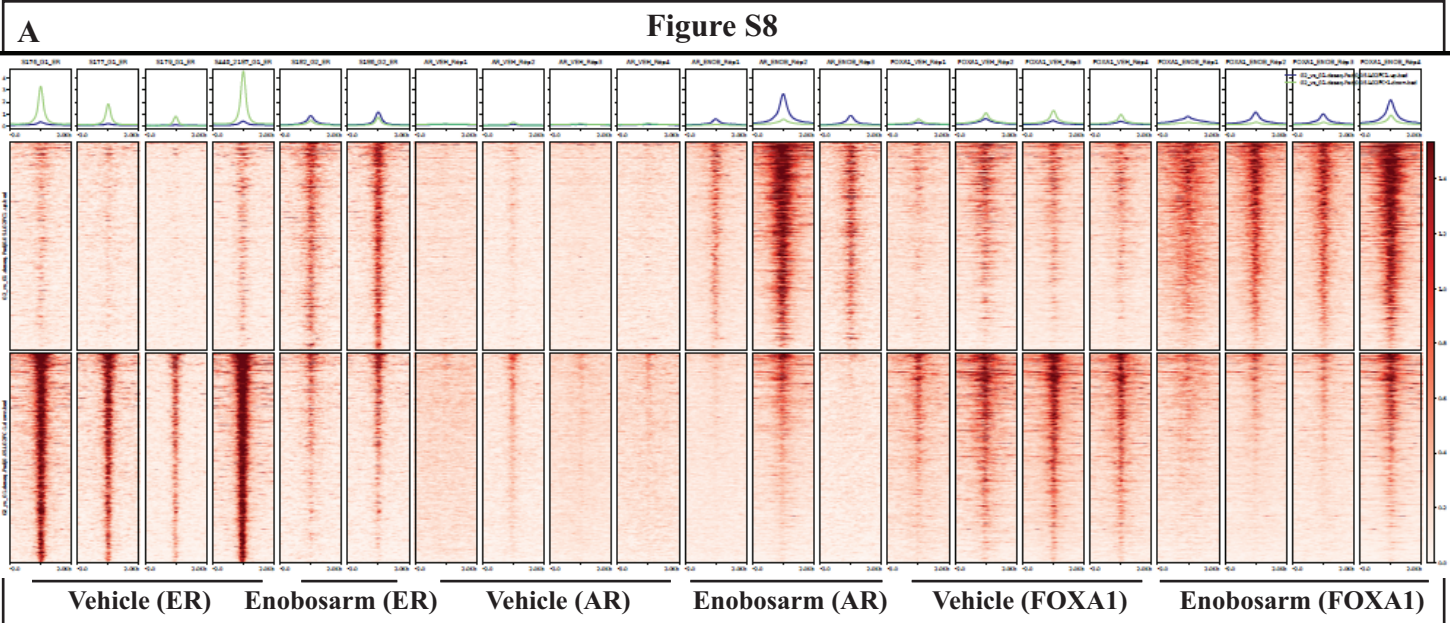

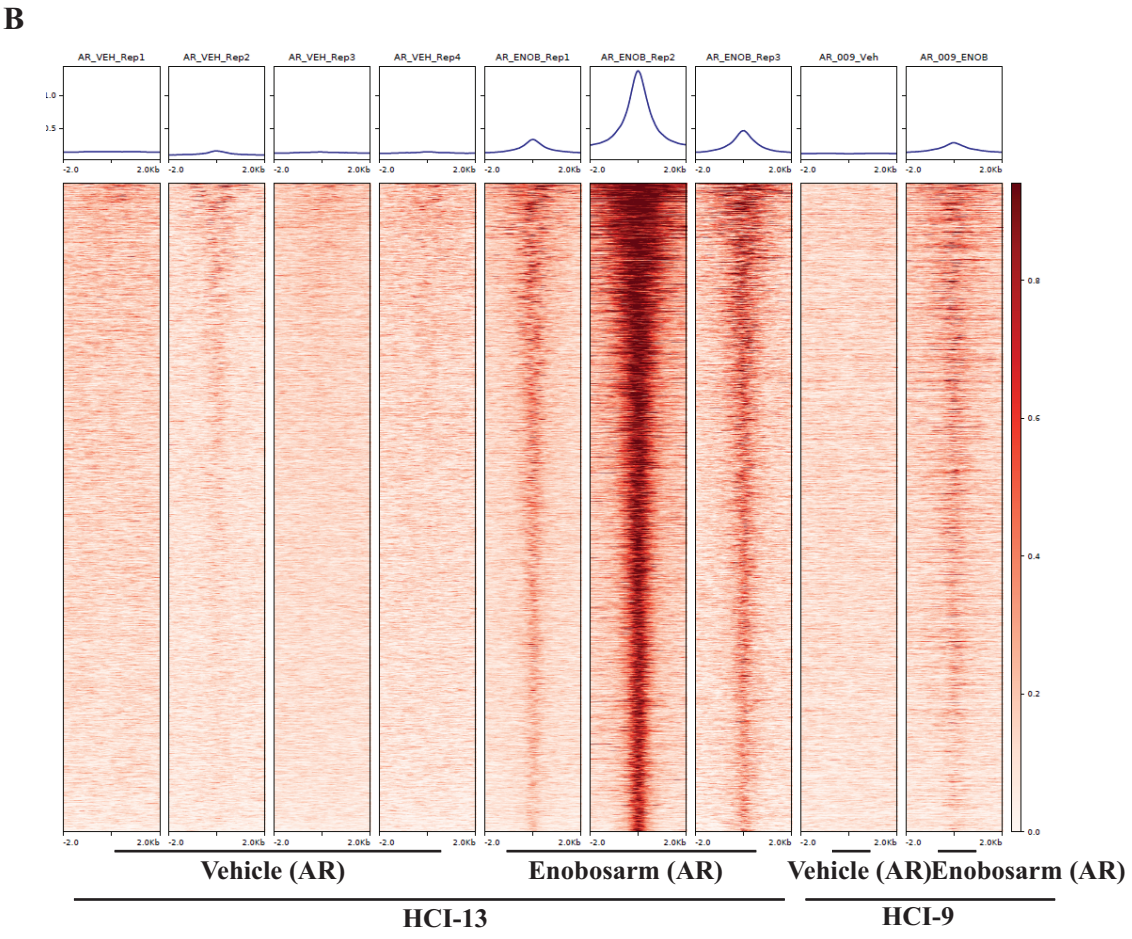

Figure S8: ER, AR, and FOXA1 DNA binding comparison (Related to Figures 3,4,5, and 7). **A**. DNA sequences that were statistically significantly enriched with or depleted of ER in enobosarm-treated samples were aligned to the same regions in AR and ER ChIP-Seq reads and represented as heatmap. **B**. ChIP-Seq for AR in HCI-9 compared to the AR enriched peaks in HCI-13.

Figure S9

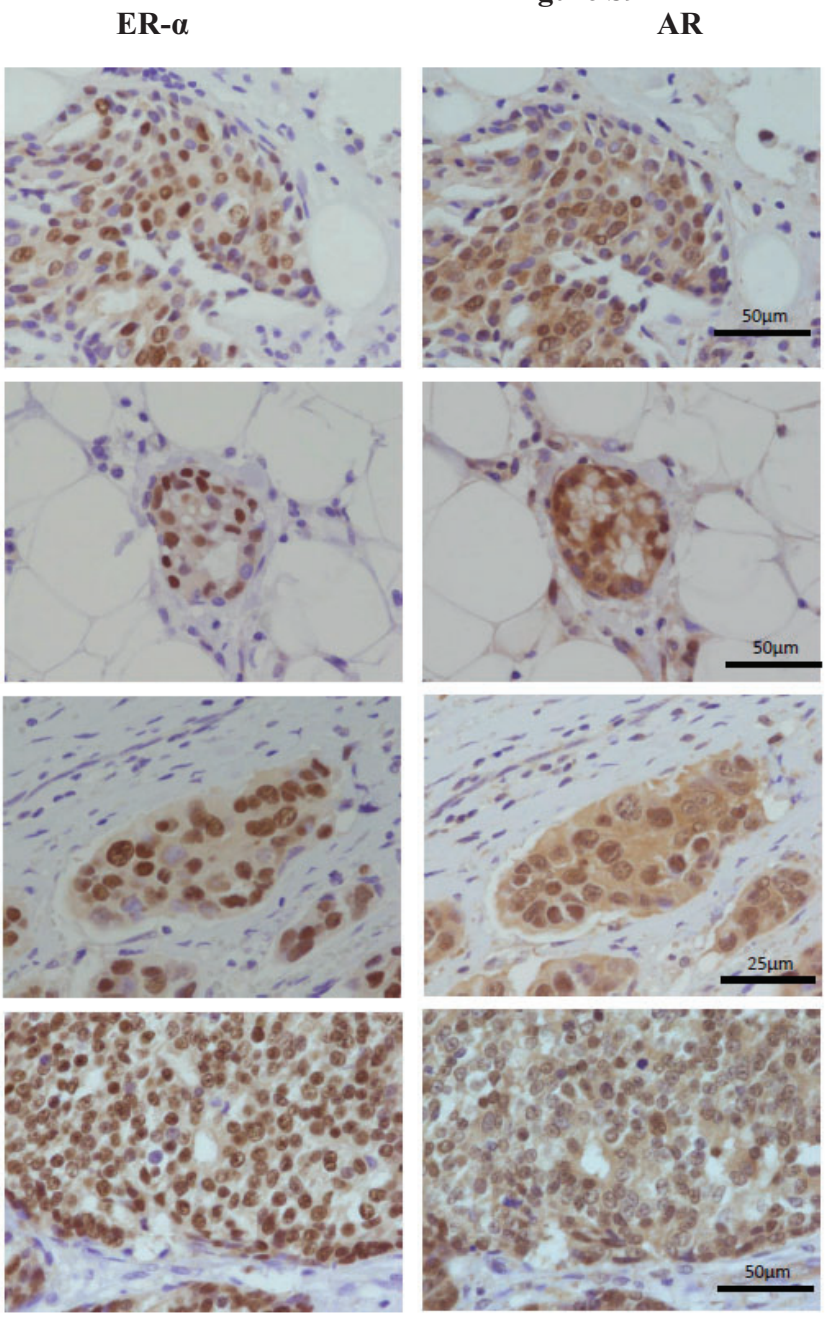

Figure S9: Colocalization of AR and ER in luminal B breast cancer specimens (Related to Figures 3 and 4). The scales are provided in each image (25 or 50 µm).

Figure S10

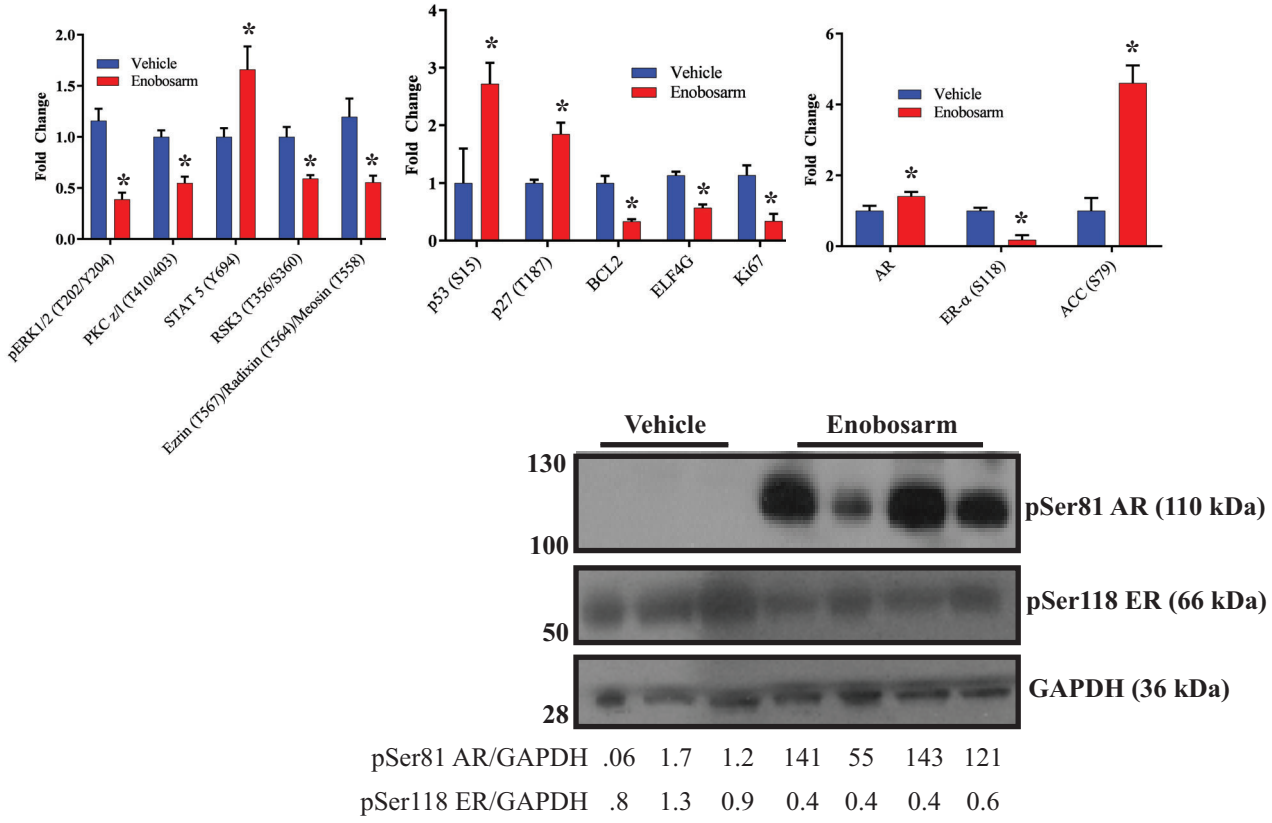

Figure S10: RPPA-based protein pathway activation analysis of HCI-13 PDX (Related to Figure 1). **A**. Lysates from HCI-13 tumor specimens (n=4) from PDX (**Figure 2B**) were printed onto nitrocellulose coated slides. Arrays were probed with a total of 174 antibodies targeting a wide range of protein kinases and their activation via phosphorylation. Arrays were stained with an anti-rabbit or anti-mouse biotinylated secondary antibody. The signals were amplified and a streptavidin-conjugated IRDye680 were used as signal detection methods. Images were acquired and quantified. Western blots were performed in the vehicle and enobosarm- treated samples to validate the results obtained with the RPPA. * $p<0.05$ from vehicle-treated samples; # $p<0.05$ from enobosarm-treated samples. n=3/group (each sample is obtained from 5 individual fragments. PDX-patient-derived xenograft; HCI-Huntsman cancer institute.

Table ST1

Patient ID	ER (%)	PR (%)	HER2 (of 3)	Ki-67 (%)	Type	Treatments prior to sample collection
1005	90	90	1+	12	Adenocarcinoma	No previous treatment
1075	30	10	N.D.	70	Invasive ductal carcinoma	Neoadjuvant (taxol)
1074	90	N.D.	0-1+	19	Invasive lobular carcinoma	Radiation, tamoxifen
1073	95	95	1+/3+	8	Infiltrating ductal carcinoma	No previous treatment
1053	100	0	3+	N.D.	Infiltrating lobular carcinoma	Taxol, Herceptin
1050	100	84	0	N.D.	Infiltrating ductal carcinoma	No previous treatment
1045	100	90	N.D.	N.D.	Infiltrating lobular carcinoma	No previous treatment
HCI-13	+	+	+		Infiltrating lobular carcinoma. Bone, brain, lung, pericardium, liver mets	Leuprolide, letrozole, exemestane, tamoxifen, zoledronic acid, cyclophosphamide, methotrexate, 5-fluorouracil, paclitaxel, doxorubicin, carboplatin, gemcitabine
HCI-7	+	+	+	N.D.	Luminal B	Paclitaxel, doxorubicin, gemcitabine, carboplatin
HCI-9	-	-	-	N.D.	Poorly differentiated adenocarcinoma	Cyclophosphamide, paclitaxel, 5-fluorouracil, anastrazole, fulvestrant, zolendronic acid

N.D. Not Done

Supplementary Table ST1 (Related to Figure 1): Characteristics of patient specimens used in preclinical studies.